Contrib Mineral Petrol (2014) 167:982
DOI 10.1007/s00410-014-0982-x

ORIGINAL PAPER

The effect of deformation on the TitaniQ geothermobarometer: an experimental study

Marianne Negrini · Holger Stunitz · Alfons Berger · Luiz F. G. Morales

Received: 6 March 2013 / Accepted: 4 February 2014 / Published online: 19 February 2014

Abstract We performed high strain (up to 47 %) axial compression experiments on natural quartz single crystals with added rutile powder (TiO_2) and $\sim$0.2 wt% H_2O to investigate the effects of deformation on the titanium-in-quartz (TitaniQ) geothermobarometer. One of the objectives was to study the relationships between different deformation mechanisms and incorporation of Ti into recrystallized quartz grains. Experiments were performed in a Griggs-type solid-medium deformation apparatus at confining pressures of 1.0–1.5 GPa and temperatures of 800–1,000 °C, at constant strain rates of 1×10^{-6} or 1×10^{-7} s^{-1}. Mobility of Ti in the fluid phase and saturation of rutile at grain boundaries during the deformation experiments are indicated by precipitation of secondary rutile in cracks and along the grain boundaries of newly recrystallized quartz grains. Microstructural analysis by light and scanning electron microscopy (the latter including electron backscatter diffraction mapping of grain misorientations) shows that the strongly deformed quartz single crystals contain a wide variety of deformation microstructures and shows evidence for subgrain rotation (SGR) and grain boundary migration recrystallization (GBMR). In addition, substantial grain growth occurred in annealing experiments after deformation. The GBMR and grain growth are evidence of moving grain boundaries, a microstructure favored by high temperatures. Electron microprobe analysis shows no significant increase in Ti content in recrystallized quartz grains formed by SGR or by GBMR, nor in grains grown by annealing. This result indicates that neither SGR nor moving grain boundaries during GBMR and grain growth are adequate processes to facilitate re-equilibration of the Ti content in experimentally deformed quartz crystals at the investigated conditions. More generally, our results suggest that exchange of Ti in quartz at low H_2O contents (which may be realistic for natural deformation conditions) is still not fully understood. Thus, the application of the TitaniQ geothermobarometer to deformed metamorphic rocks at low fluid contents may not be as straightforward as previously thought and requires further research.

Keywords Quartz · TitaniQ · Thermobarometry · Experiments · Recrystallization mechanisms

Communicated by J. Hoefs.

M. Negrini (✉) · H. Stunitz
Institute for Geology, University of Tromsø, 9037 Tromsø, Norway
e-mail: marianne.negrini@uit.no

A. Berger
Department of Geography og Geology, 1350 Copenhagen, Denmark

L. F. G. Morales
GFZ German Research Center for Geosciences, Section 3.2, 14473 Potsdam, Germany

Introduction

The reconstruction of metamorphic pressure–temperature (*P–T*) paths, especially in conjunction with the deformation history of rocks, is one of the primary tasks of tectonics and structural geology research. The pressures and temperatures of deformation can in some cases be determined with a reasonable degree of accuracy, based on the chemistry of coexisting mineral phases (conventional thermobarometry) or by thermodynamic modeling based on the properties of minerals (*P–T–X* pseudosections). However, the fact that derived pressures and temperatures indicate the ambient

P,*T* conditions of a given deformation event can only be established if the synkinematic nature of the mineral assemblage is demonstrated. The relationship between deformation and metamorphic reactions is not always straightforward or easy to establish.

New geothermobarometers (such as TitaniQ, Ti in Olivine), which are based on the chemical composition (trace elements) of a single phase, have the potential to determine the temperature and pressure of deformation directly (Kohn and Northrup 2009) if the trace element content is reset by, e.g., dynamic recrystallization during deformation. The simplicity of a trace element geothermobarometer offers a large number of new insights into geological processes.

The geothermobarometer titanium-in-quartz (TitaniQ), based on the temperature (Wark and Watson 2006; Ostapenko et al. 2007) and pressure dependence (Thomas et al. 2010) of Titanium (Ti^{4+}) substitution for tetrahedral Silicon (Si^{4+}), has a high potential to record local temperatures in a major rock forming mineral (quartz). Since its introduction, it has been successfully applied to the analysis of plutonic rocks (e.g., Kawasaki and Osanai 2008; Jacamon and Larsen 2009; Huang and Audétat 2012), volcanic rhyolites (e.g., Wark et al. 2007; Campbell et al. 2009; Vazquez et al. 2009; Girard and Stix 2010; Smith et al. 2010; Wilson et al. 2012) and hydrothermal quartzite (e.g., Rusk 2006; Rusk et al. 2008; Barker et al. 2010).

In contrast to well-equilibrated systems, the equilibration of Ti in metamorphic and deformed rocks is less clear. Several *P*–*T* determinations using the TitaniQ geothermobarometer on deformed quartz are in good agreement with data obtained from other geothermobarometers (e.g., Vazquez et al. 2009; Campbell et al. 2009; Menegon et al. 2011; Huang and Audétat 2012), whereas other studies reported discrepancies between the *P*–*T* data obtained with the TitaniQ and other geothermobarometers (e.g., Grujic et al. 2011; Wilson et al. 2012). Conflicting results may arise from the lack of knowledge on how deformation and recrystallization processes may affect the Ti–Si substitution in quartz. Grujic et al. (2011) and Härtel and Herweg (2013) have studied, based on natural samples, the effects of recovery and recrystallization on resetting the TitaniQ geothermobarometer. These authors suggest that grain boundary migration recrystallization (GBMR) (active at temperatures >500 °C) resets the Ti content in the recrystallized quartz grains, whereas rotation recrystallization occurring at lower temperatures does not. This observation challenges the earlier work of Kohn and Northrup (2009), who suggested that the temperatures of mylonitization can be determined using TitaniQ even at relatively low temperatures. In addition, deformation may influence the solid-state diffusion process compromising the applicability of the TitaniQ (which has been calibrated at static conditions) to rocks that experienced dynamic deformation. Variable Ti diffusion rates in different quartz grains have been reported by Spear and Wark (2009) and Storm and Spear (2009).

Previous studies, which relate TitaniQ-derived *P*–*T* conditions to the deformation history, have been based on field observations. However, the analysis of natural samples can be inconclusive as many factors (e.g., Ti-activity (a_{Ti}), water content during deformation, strain rate and preexisting Ti content) are unknown. Therefore, laboratory experiments performed under controlled conditions are needed for understanding the processes of Ti incorporation into quartz grains during deformation conditions.

The aim of this work was to study experimentally the effects of different recrystallization mechanisms (bulging recrystallization, subgrain rotation recrystallization, GBMR) on the mobilization, incorporation and resetting of Ti in quartz. We performed deformation experiments on quartz single crystals in the presence of Ti using a modified Griggs-type solid-medium deformation apparatus over a range of conditions that favor the activity of different deformation regimes and recrystallization mechanisms in quartz (Hirth and Tullis 1992; Stipp et al. 2002a, b). Microstructural observations are directly compared to trace element analyses in order to study the incorporation of Ti in dynamically recrystallized quartz.

Element exchange and dynamic recrystallization

Geothermobarometry is based on the amount of elements that are incorporated in a mineral at equilibrium conditions. The incorporation of elements in a mineral can either occur as ionic substitution during grain growth or by (subsequent) solid-state diffusion. In order to determine the *P*,*T* conditions of a mineral by geothermobarometry, it is necessary to assume that the mineral composition has not been modified by diffusion after equilibration at the temperature and pressure conditions of interest. Cherniak et al. (2007) have determined D-values for Ti diffusion in Quartz of 3×10^{-26} and $\sim 1.3 \times 10^{-22}$ m^2 s^{-1} for temperatures of 500 and 700 °C, respectively. The "characteristic transport distance" ($[4Dt]^{1/2}$) over which Ti may diffuse at 500 °C is ~ 2 μm in 1 m.y.; at 700 °C, this distance increases to ~ 125 μm for the same period. Due to the slow diffusion of Ti in quartz, it is to be expected that in experiments (which run for a few days), the incorporation of trace elements occurs only by ionic substitution during grain growth. The incorporation of Ti in quartz crystallized and grown from a fluid has been clearly demonstrated and documented by previous experiments conducted in piston–cylinder apparatus at static conditions (e.g., Wark and Watson 2006; Thomas et al. 2010). However, there has been no

systematic study on the incorporation of Ti in quartz during dynamic recrystallization in a deforming system.

In order to assess the Ti exchange mechanisms during deformation, it is necessary to briefly review the most important processes of dynamic recrystallization and their potential effect on ionic exchange. Two main processes occur during dynamic recrystallization: (1) progressive subgrain rotation (SGR) and (2) grain boundary migration (GBM). During SGR, vacancies move through the crystal structure and allow to climb of line defects (dislocations), which become arranged in low angle (=subgrain) boundaries (e.g., Poirier 1985). As climb is facilitated by volume diffusion of vacancies, the process of SGR is a volume diffusion-dependent process and takes place entirely within the original quartz grain. Ti exchange during SGR is expected to be controlled by volume diffusion coefficients as determined by Cherniak et al. (2007).

The second process, GBM, is the movement of a grain boundary across a grain. During dynamic recrystallization, the driving potential for boundary movement is inferred to be a local difference in dislocation density (e.g., Guillope and Poirier 1979; Poirier 1985). The dislocations constitute stored strain energy in the crystal, and therefore, this type of boundary migration is called strain-induced grain boundary migration (SIGM). During GBM, atoms move from one crystal structure to the next across the grain boundary region. If a fluid film is present along the boundary, the process involves dissolution of ions from one crystal, transport in the boundary fluid film and precipitation on another crystal. During GBM, a change in chemical composition of the crystal may occur in the wake of the moving boundary leading to the formation of a solid solution (Hay and Evans 1987a, b). The driving potential for the boundary migration will in part be the lowering of the free energy by the solid solution formation. This process is called chemically induced grain boundary migration (CIGM) or diffusion-induced grain boundary migration (DIGM; Evans et al. 1986; Hay and Evans 1987a, b, and references therein). We will use the term CIGM in this contribution. The solute (=Ti in the case of Ti exchange in quartz) is transported along the moving boundary by grain boundary diffusion or diffusion in the fluid and subsequently incorporated in the growing crystal (Hay and Evans 1987a, b, their Fig. 1). The process typically occurs at homologous temperatures T/T_m of 0.3–0.7 in experiments (i.e., at relatively low temperatures; Hay and Evans 1987a, b), and the chemical change by CIGM may be orders of magnitude faster than by volume diffusion.

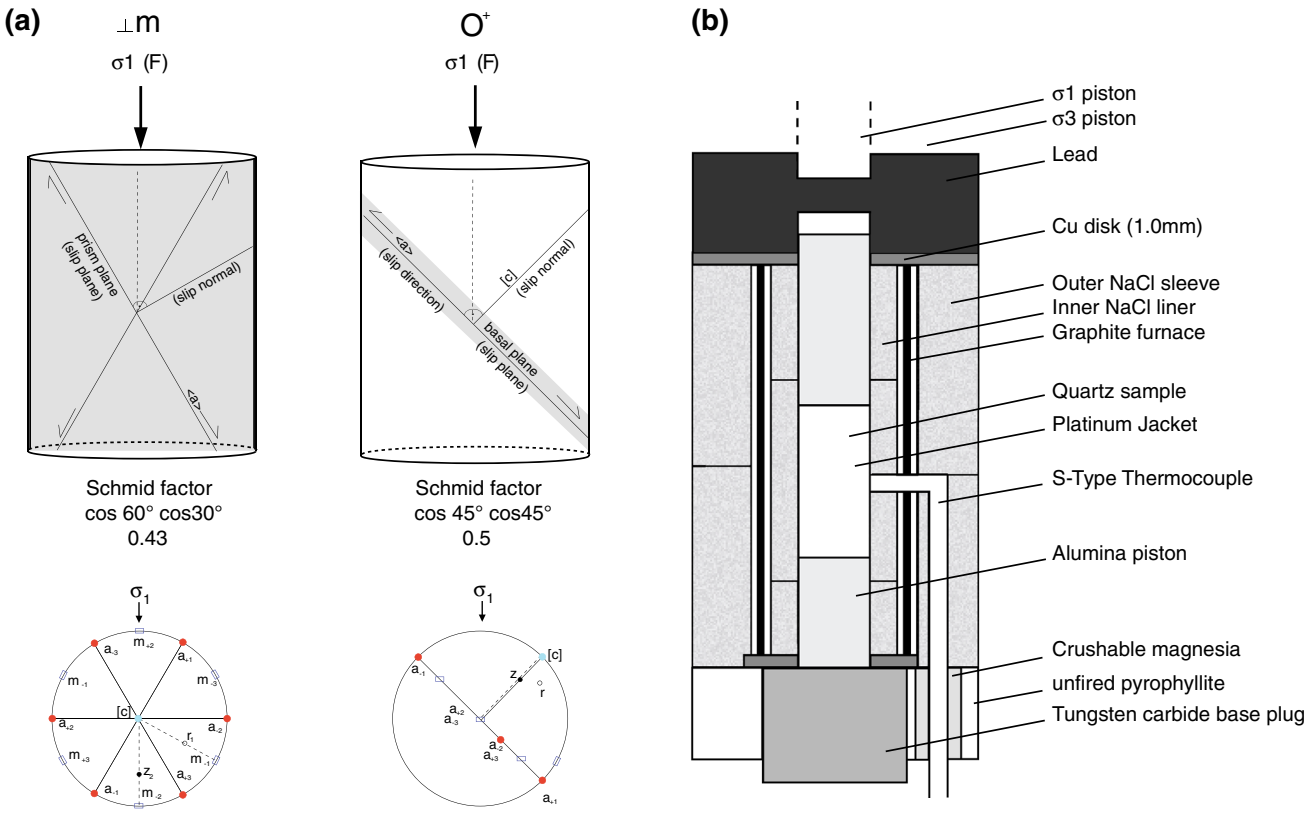

Fig. 1 **a** Schematic representation and stereographic projection of the sample orientations used in the experiments, (*left*) normal {m} and (*right*) O^+ orientation (modified after Thust et al. 2012). **b** Schematic drawing of the sample assembly used in this study for the deformation experiments performed in a Griggs-type solid-medium deformation apparatus. Modified after Tarantola et al. (2010)

Although the occurrence of CIGM is demonstrated in experiments, its driving potential is not entirely resolved (Hay and Evans 1987a, b), and with the difficulty of determining dislocation densities in deforming minerals, it is unclear whether the GBM process in deforming quartz during syndeformational recrystallization is dominantly SIGM or CIGM (Stünitz 1998). In any case, the GBM process is expected to exchange Ti in quartz many orders of magnitude faster than volume diffusion of Ti, which is the rate-controlling process for Ti exchange during recrystallization by SGR (see also Grujic et al. 2011; Härtel and Herweg 2013). Likewise, grain growth (during, for example, static recrystallization processes) also involves the migration of grain boundaries, and ionic exchange through the moving boundaries and/or grain boundary fluids is expected.

Methods

Starting material

The starting material for all experiments was cored from a euhedral natural quartz single crystal from a vein in the Aar Massif, Central Alps, Switzerland. Macroscopically, the quartz crystal shows some inhomogeneity in the form of randomly distributed milky regions. The varying opacity (milkyness) of the crystal is caused by the presence of H_2O-rich fluid inclusions with lengths of up to 200 μm. For our experiments, the milky regions of the quartz crystal were chosen, because the experiments require the presence of aqueous fluid during deformation. The clear quartz, where no fluid inclusions are observed, is essentially dry, whereas the water content of the milky regions is strongly inhomogeneous and depends on the size and distribution of the fluid inclusions (Thust et al. 2012). Further information concerning the nature and distribution of the fluid inclusions, as well as mechanical and physical properties of the quartz crystal, can be found in Tarantola et al. (2012) and Thust et al. (2012).

Light microscope observations show that the quartz crystal is optically strain-free and that it contains no solid impurities. In particular, no rutile inclusions were observed. Electron microprobe analyses (EMPA; analytical methods described below) of the quartz crystal reveal uniform Ti contents below the detection limit of the EPMA of 20 ppm.

Single-crystal material was chosen instead of polycrystalline material in order to unequivocally identify new grains formed during the deformation process. In polycrystalline material, deformation may lead to nucleation and growth of new grains, but these are often difficult to distinguish from the original grains. In addition, Ti measurements in fine-grained aggregates are difficult as Ti-rich phases, such as rutile inclusions, may be present along the grain boundaries and could (due to the spatial resolution of the electron microprobe) be included in the analysis and influence the results.

Sample preparation

We used two sets of samples during the experiments (Fig. 1a) cored in two crystallographic orientations in order to produce different recrystallization microstructures by activating different slip systems. The O^+ sample set, where slip occurs along the basal <a> and prism <c> slip systems, was cored at 45° to the basal plane and to the *c*-axis of the quartz crystal (e.g., Baeta and Ashbee 1969a, b; Blacic and Christie 1984; Tarantola et al. 2010; Fig. 1a). The normal {m} set ($_{\perp}$m), where slip occurs along the prism <a> slip system, was cored with the *c*-axis, and one of the prism planes normal to the sample cylinder axis (Fig. 1a).

All samples had a diameter of 6.3 mm and a length ranging from 10 to 12 mm. Two different sample arrangements were used: Some samples consisted of a single cylinder, while in others, we placed two short (5–6 mm) cylinders on top of each other in order to increase the amount of added TiO_2 powder, to better distribute the powder in the sample and to increase the surface area which is in contact with the TiO_2 powder.

The quartz cylinders were placed in a pre-annealed platinum (Pt) jacket, and 0.01–0.03 g of fine-grained TiO_2 powder was evenly placed around the quartz cylinders. In samples formed by two cylinders, TiO_2 powder was also placed in between the two cylinders. Distilled H_2O (0.1–0.3 μl) was added with a micropipette to the lower part of the sample in order to prevent evaporation during the welding of the Pt-jacket. Mechanical welding was performed with a Lambert welding device using a millisecond welding time to minimize heating of the sample. All the samples were sandwiched between two Al_2O_3 pistons and placed in the center of a graphite furnace. In all experiments, we used sodium chloride (NaCl) liners as the solid confining medium. The sample assembly used in the experiments is illustrated in Fig. 1b.

Experimental setup

High strain (up to 47 %) axial compression experiments were performed with a modified Griggs-type solid-medium deformation apparatus (Griggs 1967; Tullis and Tullis 1986) at pressures of 1.0–1.5 GPa, temperatures ranging from 800 to 1,000 °C, and constant strain rates of 10^{-6} and 10^{-7} s^{-1}. An overview of experimental conditions is presented in Table 1. As one of the main aims of the

Table 1 Deformation conditions (Pc = confining pressure, T = temperature, strain rate, deformation time and total strain) and sample parameters (sample orientation, added TiO_2 and added H_2O) of all deformation experiments

Sample	Pc (GPa)	T (°C)	Strain rate (10^{-6} s^{-1})	Time (h)				Strain (%)	Experiment type	Orientation	TiO_2(g)	H_2O (µl)
				before hit point	deformation	annealing	total time					
mn273	1.00	900	0	26	0	0	26	0	Hydrostatic	$_{\perp}$m	0.01	0.1
mn275	1.00	900	1.4	58	60	0	118	32	Axial	$_{\perp}$m	0.01	0.1
mn277	1.00	800	1.4	24	88	0	112	47	Axial	$_{\perp}$m	0.01	0.1
mn299	1.00	900	1.2	33	80	0	113	37	Axial	O^+	0.01	0.1
mn301	1.50	1,000	1.4	0	90	0	90	28	Axial/prehit	O^+	0.01	0.1
mn319	1.50	900	1.2	36	99	76	211	47	Axial	O^+	0.02	0.1
mn321	1.20	1,000	1.1	24	30	0	54	16	Axial/prehit	O^+	0.01	0.1
mn326	1.50	1,000	1.4	67	93	0	160	40	Axial	$_{\perp}$m	0.03	0.1
mn331	1.50	1,000	0.1	42	244	0	286	20	Axial	$_{\perp}$m	0.02	0.3
mn332	1.50	1,000	1.4	0	120	139	259	20	Axial	$_{\perp}$m	0.02	0.3

experiments was to study the effects of different recrystallization mechanisms on re-equilibration of the Ti content in quartz, the range of experimental conditions was chosen in an attempt to activate both subgrain rotation recrystallization and grain boundary migration recrystallization in quartz according to the conditions determined by Hirth and Tullis (1992) and Stipp et al. (2002a, b). We use the Thomas et al. (2010) calibration for expected equilibrium Ti values in quartz and Hirth and Tullis (1992) for deformation regimes in quartz (Table 2).

During each experiment, confining pressure and temperature were increased in a step-wise manner until the desired deformation conditions were reached, typically in ~8 h. As the samples were fluid bearing, heating was started after reaching confining pressures (Pc) of at least 0.2 GPa in order to minimize the internal pressure of the capsule. Temperature was increased in steps of 100 °C at a rate of 25 °C per minute. Temperature was monitored with a Pt–Pt10 %Rh S-type thermocouple placed in the center of the sample. In order to verify the thermal gradient in the sample during deformation, a double thermocouple experiment was performed in which one thermocouple was placed in the center and the other at the lower end of the sample. The results of this test show a maximum temperature difference of ~10 % from the center of the sample to the alumina piston (a distance of ~6 mm).

After reaching the desired conditions, deformation was started by advancing the axial piston (σ_1) at a constant strain rate (10^{-6} or 10^{-7} s^{-1}). During deformation, mechanical data (force applied to the sample, displacement of the piston, confining pressure and external room temperature) were registered at 1-s intervals. Once the desired total strain was achieved, temperature was quenched to 200 °C in 2 min or less in most experiments in order to preserve the deformation microstructures. In two deformation experiments, temperatures were held after deformation at 900 °C for 76 h (mn319) and 1,000 °C for 139 h (mn332) in order to induce annealing and grain growth of the recrystallized grains and thus movement of grain boundaries.

Mechanical data were processed using the Matlab program RIG (http://sites.google.com/site/rigprogram/) taking into consideration internal friction and distortion of the deformation apparatus. Differential stress was corrected for changes in sample area and confining pressure during deformation. Full details regarding corrections and evaluation of the mechanical data can be found in Pec et al. (2011).

Analytical methods

Deformed samples were cut parallel to the loading direction (parallel to the sample cylinder axis) through the middle of the sample, and polished thin sections were prepared with a thickness of 30 µm. Major and trace element analyses were performed with a JEOL Superprobe JXA 8200× at the University of Copenhagen using an acceleration voltage of 20 kV, a beam current of 200 nA, a beam diameter of 3–15 µm and counting times of 240 s on the peak and 120 s on each high and low background positions. Standardization was performed on rutile and SiO_2 using the same conditions as above. At these conditions, the given detection limit of the instrument is on average 20 ppm for Ti.

EMPA analysis was chosen instead of secondary ion mass spectrometry (SIMS) and laser ablation inductively coupled plasma mass spectrometry (LA-ICP-MS), because (1) EMPA offers the best spatial resolution (smallest interaction volume) of these methods. One of the difficulties in measuring Ti in quartz is to avoid interaction of the

Table 2 Ti content and deformation behavior expected for quartz, deformed in the temperature range 800–1,000 °C and at different confining pressures (1.0–1.5 GPa)

Experimental conditions		Expected Ti (ppm)	Deformation regime	Expected deformation mechanisms
T (°C)	p (GPa)			
800	1.0	147	2	Subgrain rotation recrystallization (SGR)
900	1.0	310	3	Grain boundaries migration (GBM) + SGR
900	1.5	127	3	Grain boundaries migration (GBM) + SGR
1,000	1.5	256	3	Grain boundaries migration (GBM) + SGR

Ti content calculated as follows: RT ln $X_{TiO2}^{quartz} = -60{,}952 + 1.520 * T(K) - 1{,}741 * p$ (kbar) + RT ln a TiO_2 (Thomas et al. 2010), where a TiO_2 was =1 because rutile is present in all samples, $R = 8.3145$ J/K (gas constant), T is temperature in °K, and p is confining pressure in kbar. To convert X_{TiO2}^{quartz} into Ti (ppm), the formula of Thomas et al. (2010) was used. Expected deformation regime and deformation mechanisms based on the experimental work of Hirth and Tullis (1992)

measuring beam with the grain boundary regions, which are sites of potential rutile precipitation. In our case, EMPA allowed measurements of the internal parts of grains and near grain boundaries of small (several μm) recrystallized grains. (2) At the chosen experimental conditions, the expected equilibrium Ti values in quartz are high (varying from 127 to 310 ppm; Table 2) and well above the detection limit of the microprobe (20 ppm Ti), and in a range of sufficient quantitative resolution for the purpose of this study.

As reported previously (Bastin et al. 1984; Hermann et al. 2005; Wark and Watson 2006; Fournelle 2007; Donovan et al. 2011), Ti contents measured by EMPA have to be treated with care because of the "phantom" Ti content (caused by secondary fluorescence, e.g., Wark and Watson 2006; Hayden and Watson 2007; Sato and Santosh 2007), which causes erroneously high apparent Ti concentrations in quartz in the vicinity of Ti-phases. These effects are observed in the samples analyzed here (e.g., Figs. 2b, 5c, 6b, 9a). The element distribution maps (Figs. 2b, 6b) of the deformed quartz single crystals show spurious Ti-haloes around rutile inclusions and locally along cracks that developed in the quartz crystals during deformation. EMPA point measurements along the spurious haloes show high apparent Ti contents (thousands of ppm), and an interaction distance varying from 100 μm in zones adjacent to large rutile aggregates to a few μm around small rutile inclusions (Fig. 2c). As proposed by Cherniak et al. (2007), volume diffusion of Ti in quartz is very slow and negligible in our short experiments (1–11 days). Thus, the observed high apparent Ti contents around rutile grains arise from fluorescence effects and therefore have to be considered as an analytical artifact (see Figs. 5c, 9a). For this work, however, phantom Ti content does not present a significant problem, because the high Ti values can always be correlated with detectable rutile inclusions or fine-grained rutile precipitates along grain boundaries. Furthermore, as is shown below, Ti contents in all cases are lower than the expected equilibrium values and any correction for "phantom" Ti in quartz would result in even lower values.

Initial microstructural observations of the deformed samples were made with a polarization light microscope. Crystallographic preferred orientation (CPO) analysis of selected samples was carried out using electron backscatter diffraction (EBSD; Adams et al.1993; Prior et al. 1999) in a scanning electron microscope. For EBSD analysis, we used a FEI Quanta 3D FEG dual-beam machine equipped with an EDAX–TSL Digiview IV EBSD detector and TSL–OIM system (v. 5.31) installed at the GFZ-Potsdam. After the standard polishing procedure, the thin sections were chemically polished using a soft cloth and an alkaline solution of colloidal silica (SYTON) (Fynn and Powell 1979) for about 3 h in order to remove damages and defects of the section surface caused by the mechanical polishing. The analyses were conducted under low vacuum (10 Pa of H_2O) allowing the use of uncoated samples. For automatic mapping of crystallographic orientations, the following parameters were used: 15 kV accelerating voltage; 8 nA beam current; 12 mm working distance; step size of 1 μm and 70° sample tilt. Post-acquisition treatment included standardization of the confidence index (CI) of different points and CI correlation between neighboring points. Only data with CI > 0.2 were considered for further analysis. The pseudohexagonal symmetry effect on quartz caused by a rotation of 60° around [0001] was also corrected.

Results

Sample deformed at 800 °C and confining pressure of 1.0 GPa

The quartz sample deformed up to a strain of 47 % shows a peak strength of 750 MPa, followed by pronounced weakening to ~400 MPa (sample mn277, Fig. 3). The heterogeneously deformed single crystal displays a wide range of deformation microstructures (Fig. 4). Strain is mainly accommodated along conjugate deformation bands

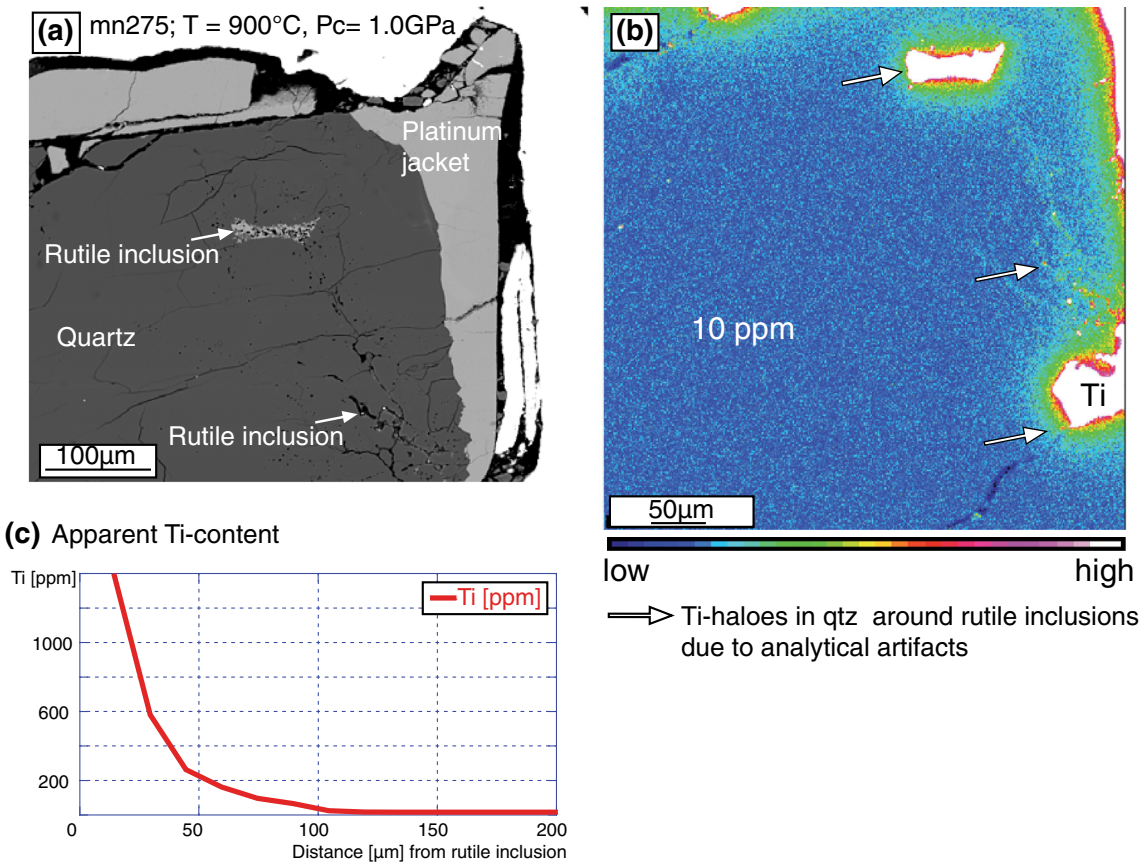

Fig. 2 Apparent spurious Ti content in quartz (see Hermann et al. 2005) around rutile inclusions in sample mn275 deformed in presence of TiO_2 powder and fluid (H_2O) at 900 °C, 1.0 GPa. **a** Backscatter image of a large rutile inclusion formed inside the quartz single crystal during deformation and recrystallization. The 100-µm-long inclusion consists of randomly oriented, 10-µm-long needles of rutile. Small rutile inclusions are found also along cracks (*arrows*). **b** Element distribution map showing the effect of spurious Ti in quartz around the rutile inclusion and the sample boundary due to the presence of phantom Ti in quartz. The Ti scale threshold was chosen in order to highlight the analytical artifacts and therefore cannot been linearly related to Ti contents measured in the sample. The distortion of the element map is caused by a difference in the imaging systems of the microprobe. **c** Spurious Ti content caused by phantom Ti in quartz. The effect is noticeable up to 100 µm distance from the rutile for large inclusions. Therefore, all measurements taken closer than 100 µm from large rutile grains are subject to error

(Fig. 4a), which extend from the piston edges and intersect in the center of the sample. Within the deformation bands, large (100–200 µm) porphyroclasts of relict quartz grains with undulatory extinction are surrounded by domains of small, recrystallized grains (Fig. 4b–d). Light microscope observations indicate the presence of small solid inclusions (probably rutile) along the boundaries of the newly recrystallized grains. Undulatory extinction of the large porphyroclasts is caused by a slight change of crystal orientation visible in the orientation map (Fig. 4c). The grain boundary misorientation map produced by EBSD (Fig. 4d) shows a high density of low angle (5–15°) boundaries (in red) around and within the large quartz relicts. Some boundaries delineate strongly elongated subgrains, with an elongation direction approximately normal to the compression (σ_1) direction. The newly recrystallized grains, with mean grain size ranging from 6 to 12 µm (Fig. 4f), are delineated by grain boundaries with a misorientation >15° (black lines in Fig. 4d). Many recrystallized grains have a similar size as the small subgrains with low angle boundaries (Fig. 4d). The histogram of the distribution of misorientation angles (Fig. 4e) shows a clear deviation from a random distribution and a high frequency of low misorientation angles between adjacent pairs (correlated). The small increase in frequency for misorientation angles between 50° and 60° probably represents Dauphiné twinning (60° rotation about the *c*-axis; Frondel 1962). The overall distribution of misorientation angles and the predominance of low angle grain boundaries suggest the presence of a CPO in the recrystallized domains of the sample.

EMPA analyses (Fig. 4c) indicate uniformly very low Ti contents (mainly below the 20 ppm detection limit of the instrument) throughout the entire quartz crystal. In

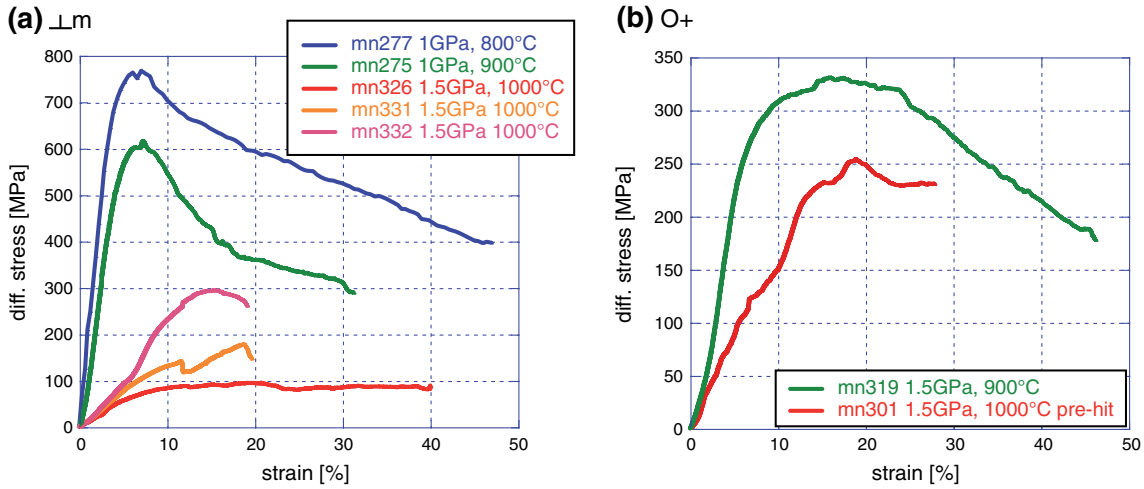

Fig. 3 Strain versus differential stress curves of samples deformed at a strain rate of 1×10^{-6} s^{-1}. Axial compression **a** normal {m} and **b** O^{+} orientation. Experiment mn301 was cracked prior deformation (pre-hit). Experiment mn331 was deformed with strain rate stepping (initially at 1×10^{-6} s^{-1} and after peak strength at 1×10^{-7} s^{-1})

addition, no systematic compositional variations between the large porphyroclasts, subgrains, small recrystallized grains and the undeformed parts of the sample were observed.

Sample deformed at 900 °C and confining pressure of 1.0 GPa

Sample mn275 (Fig. 2) deformed up to a strain of 32 % shows a similar strength development as sample mn277, with peak strength of 600 MPa followed by pronounced weakening to ~350 MPa (Fig. 3). Deformation was accommodated mainly along a conjugate set of deformation bands oriented at 50° to the compression (σ_1) direction, crosscutting the whole sample. Dominant microstructures in the sample are deformation lamellae and pronounced undulatory extinction produced by crystal lattice distortion. Backscatter SEM images (Fig. 2a) and EMPA element distribution maps (Fig. 2b) show the presence of large (100 μm), newly formed rutile aggregates in the internal parts of the quartz crystal, together with small rutile inclusions along cracks formed during the experiments (Fig. 2b). EMPA measurements indicate Ti contents below the detection limit throughout the entire quartz crystal, with the exception of the vicinity of the rutile inclusions along cracks and grain boundaries (due to analytical artifacts, see above).

Sample deformed at 900 °C and confining pressure of 1.5 GPa

Sample mn319 (O^{+} orientation) was deformed for 99 h at 900 °C and confining pressure of 1.5 GPa and then annealed at hydrostatic conditions for 76 h after deformation. The mechanical data show a peak strength of 330 MPa followed by pronounced weakening after a strain of ~25 % (Fig. 3).

The heterogeneously deformed sample shows localization of deformation into recrystallized bands oriented approximately 45° to the compression (σ_1) direction (Fig. 5a). The recrystallized bands are composed of coarse-grained domains (domain I) and fine-grained domains (domain II). The coarser-grained domains consist of grains with variable size ranging up to 65 μm (Fig. 5b–d, f), although locally grains can reach 500 μm (region 3, Figs. 5a, 6a). The large recrystallized grains, which show no undulatory extinction, have irregular to polygonal shapes and smoothly curved grain boundaries where local pinning occurs (Fig. 6a). High angle grain boundaries separate the large recrystallized grains from neighboring, strongly elongated relict porphyroclasts (Fig. 5d). The relict porphyroclasts contain subgrains of considerably smaller size (~3 to 7 μm) defined by misorientation angles of 5–15° (Fig. 5d). The size of the subgrains is similar to the size of the recrystallized grains in domain II (Fig. 5c, d, f).

A narrow but distinct zone with smaller grains is present close to the boundary of the two sample pieces (domain II in Fig. 5c, d). In this zone, the recrystallized grains show a mean grain size of ~5 μm (Fig. 5f). The histogram of the distribution of misorientation angles (correlated, red bars) (Fig. 5e) from domain II shows a high frequency of small misorientation angles. This indicates that progressive subgrain rotation is the likely recrystallization mechanism, consistent with the similar size of subgrains and recrystallized grains. The submaximum in misorientation angles

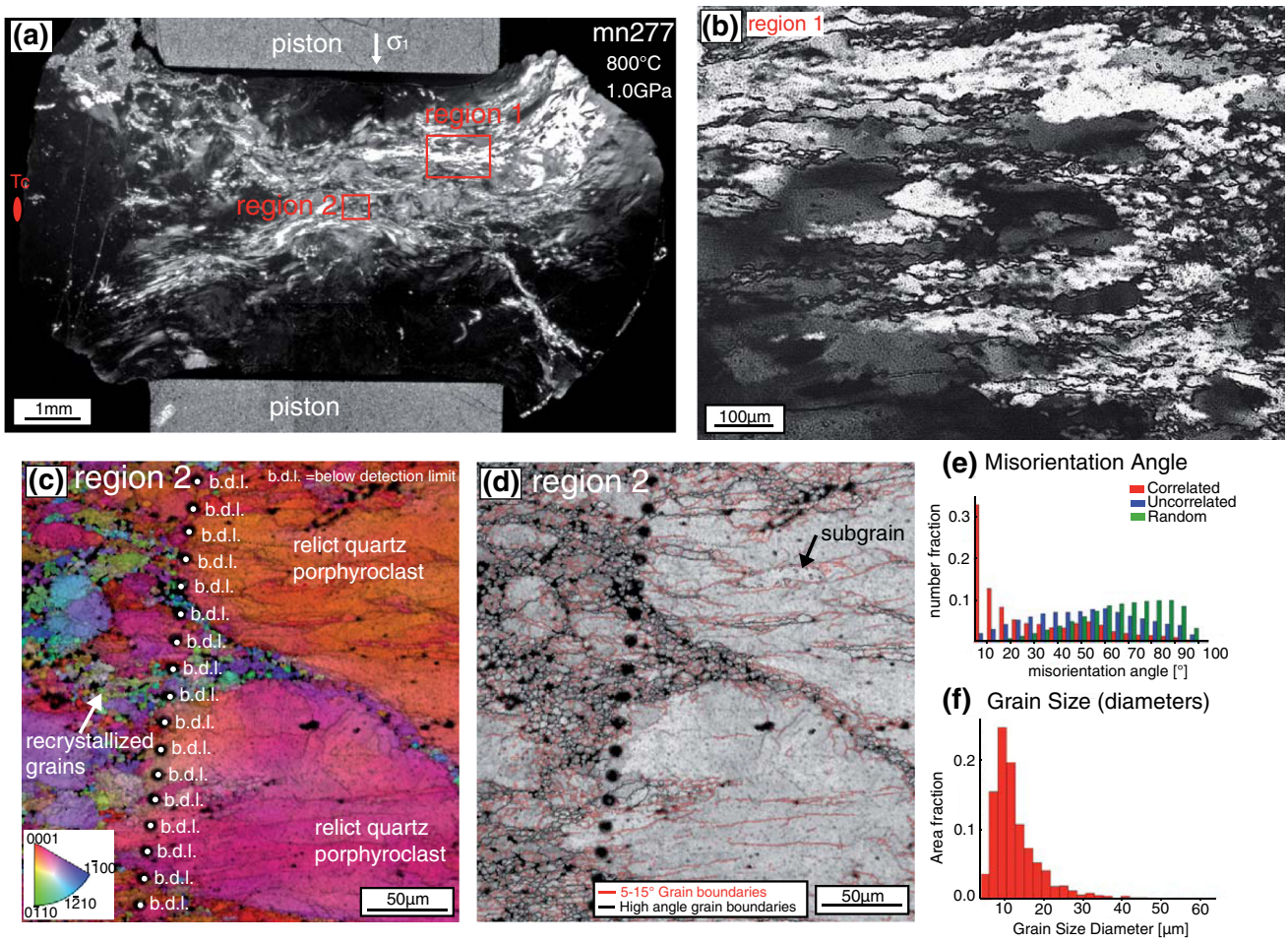

Fig. 4 Microstructures and Ti content of sample mn277 deformed to an axial strain of 47 % at a strain rate of 1×10^{-6} s^{-1}, 800 °C, 1.0 GPa in the presence of TiO_2 powder and fluid (H_2O). Compression direction is vertical in all images. **a** Light micrograph (crossed polarizers) of sample mn277. Final position of the thermocouple (Tc) and positions of the analyzed regions are marked in *red*. **b** Light micrograph (cross-polarized) of typical microstructures of a strongly deformed part of the sample (region 1). Considering the temperature gradient in the sample, deformation occurred in this region at a temperature of 795 °C. **c** EBSD orientation image of region 2. Orientations according to the inverse pole figure given in the *lower corner* of the image. *White numbers* indicate the Ti contents (ppm) measured by EPMA. The expected equilibrium Ti content at 800 °C, 1.0 GPa is 147 ppm (Thomas et al. 2010). **d** Grain boundary misorientation map of region 2 acquired with EBSD using nearest neighbor pairs. Misorientation angles of 5–15° are represented in *red*, misorientation >15° are represented in *black*. **e** Histogram of distribution of angles between nearest neighbor pixels (correlated, *red bars*) and for uncorrelated pairs (*blue bars*). Distribution for random orientation is given by *green bars*. Bins are at 5° interval. Measurements below 5° are omitted, because of inaccuracy (Kruse et al. 2001; Prior et al. 1999) **f** Grain size distribution (area fraction) of the recrystallized region 2

at 50°–60° may represent Dauphiné twin boundaries (Frondel 1962).

The bimodal grain size distribution of the whole sample is consistent with abnormal grain growth during annealing. Thus, during annealing, the population of grains with sizes of 10–65 µm and curved, polygonal grain boundaries most likely grew from the originally dynamically recrystallized grains (~3–7 µm).

EMPA measurements were performed in three different regions within the sample. Considering the temperature gradient in the sample (temperature decrease of around 10 % from center to the edges), the analyzed regions were deformed at temperatures of 894 °C (region 1 Fig. 5b), 900 °C (region 2, Fig. 5c), and 890 °C (region 3, Fig. 6). All EMPA analyses in region 1 and in domain I of region 2 show Ti concentrations below or close to the detection limit. The Ti values measured in the undeformed and recrystallized parts of this region are the same as the Ti concentration of the starting material (Figs. 5b, 6b). An EMPA element distribution map (Fig. 6) displays small rutile inclusions at grain boundaries (few µm in size). In the upper right corner of the map shown in Fig. 6, a local Ti enrichment of quartz is observed. This region is in close proximity to the sample edge, where primary rutile is

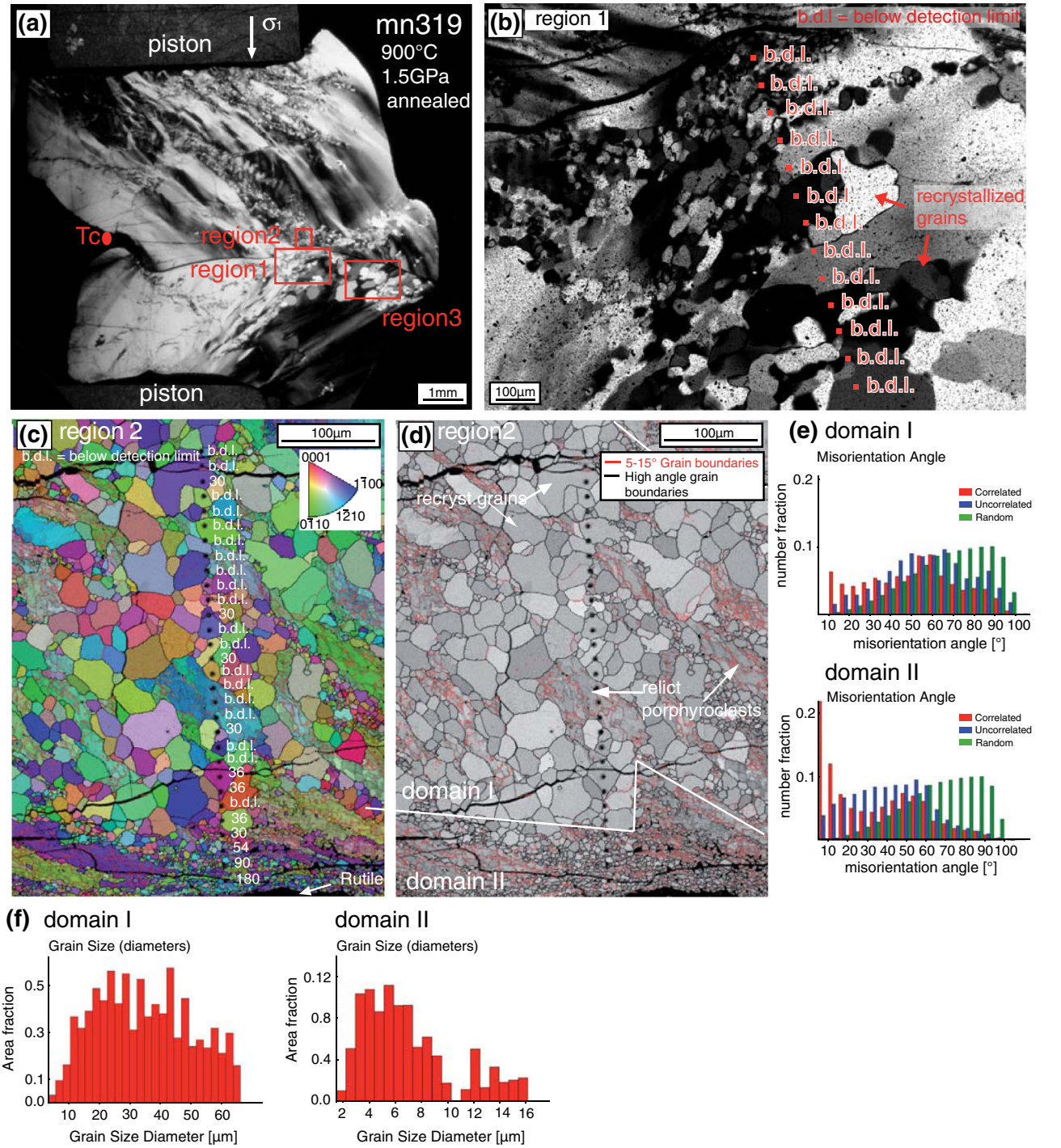

Fig. 5 Sample mn319 deformed at 900 °C, 1.5 GPa at a strain rate of 1×10^{-6} s^{-1}, in presence of TiO_2 powder and fluid (H_2O). Compression direction (σ_1) is *vertical* in all images. **a** Light micrograph (crossed polarizers) of sample mn319. Final position of the thermocouple (Tc) and position of the analyzed regions are marked in *red*. **b** Cross-polarized light micrograph of recrystallized region 1. Considering the temperature gradient in the sample, deformation occurred in this region at a temperature of 894 °C. Ti contents measured by EPMA are marked in *red* (detection limit 20 ppm). The expected equilibrium Ti content is 121 ppm. **c** EBSD orientation image of region 2 (Ti content in white numbers, expected Ti content: 127 ppm). Orientations according to the inverse pole figure given in the *upper corner* of the image. **d** Grain boundary misorientation map of region 2 acquired with EBSD using nearest neighbor pairs. Misorientation angles <15° are represented in *red*, misorientation >15° are represented in *black*. Note the two distinct grain sizes of domain I and II. **e** Histogram of distribution of misorientation angles for domain I and II. Correlated (*red bars*), uncorrelated (*blue bars*) and random (*green bars*). **f** Grain size distribution (area fraction) of domain I and II of the recrystallized region 2

present (see analytical artifacts in Methods section). In domain II of region 2, the increased Ti values in the fine-grained recrystallized quartz grains are due to phantom Ti, otherwise all Ti values are below the detection limit, except a few measurements at grain boundaries (Fig. 5c).

Samples deformed at 1,000 °C and confining pressure of 1.5 GPa

Samples deformed at a temperature of 1,000 °C and 1.5 GPa confining pressure exhibit variable mechanical behavior (Fig. 3a, b). Peak strength varies from 90 MPa of sample mn326 to 300 MPa of sample mn332. Samples mn301 and mn332 show some weakening after reaching peak strength, whereas sample mn326 achieved steady state flow (80 MPa) at relatively low strains (Fig. 3a). Sample mn331, which was deformed up to peak strength at a strain rate of 1×10^{-6} s^{-1} and then at a strain rate of 1×10^{-7} s^{-1}, shows peak strength of 180 MPa.

Sample mn301, deformed in the O^+ orientation (Fig. 7), was deliberately pre-cracked during the loading process and subsequently deformed to a strain of 28 %. This sample does not show extensive recrystallization. The initial cracking at low confining pressure produced longitudinal fractures oriented parallel to the compression direction (Fig. 7a). Subsequent crystal plastic deformation has produced bulges of the sample, together with isolated patches of recrystallized quartz aggregates (Fig. 7a–c). The patches are connected with the initial cracks and consist of grains of variable size (10–100 µm), with irregular shapes and lobate grain boundaries. The frequency distribution of misorientation angles (Fig. 7d) for neighbors and uncorrelated grains shows a more random distribution compared to lower temperature experiments. The frequency of misorientation angles <15° is lower than in experiments at 800 and 900 °C, except for the very low misorientation angles (<5°).

The chemical composition of three recrystallized patches in sample mn301 was analyzed by microprobe. Considering the relative position of the patches with respect to the final position of the thermocouple and the temperature gradient in the sample, a deformation temperature of 981 °C was calculated for region 1 (Fig. 7b), 953 °C for region 2 (Fig. 7c) and 1,000 °C for region 3 (Fig. 7e). EMPA analyses show strong variations in the Ti content for all three patches, ranging from values below the detection limit to 3,338 ppm (Fig. 7b, c, e). High Ti contents are always measured close to grain triple junctions, along grain boundaries, or along cracks (Fig. 7b, c). The element distribution map acquired in region 3 (Fig. 7f) shows high Ti values in discrete points, triple junctions of quartz grains, along cracks and in very narrow lines, all of which coincide with grain boundaries (Fig. 7e, f). Thus, Ti contents above the detection limit are only recorded from areas related to newly formed rutile precipitates on triple junctions and grain boundaries of quartz, whereas the internal parts of grains show Ti contents uniformly below or close to the detection limit of the instrument.

The microstructures of all three samples of ⊥m orientation are quite similar to each other (Fig. 8). Sample mn326 (Fig. 8a, b), which was deformed up to a strain of 40 %, shows extensive recrystallized bands surrounding relicts of more weakly deformed host quartz (Fig. 8a). The quartz

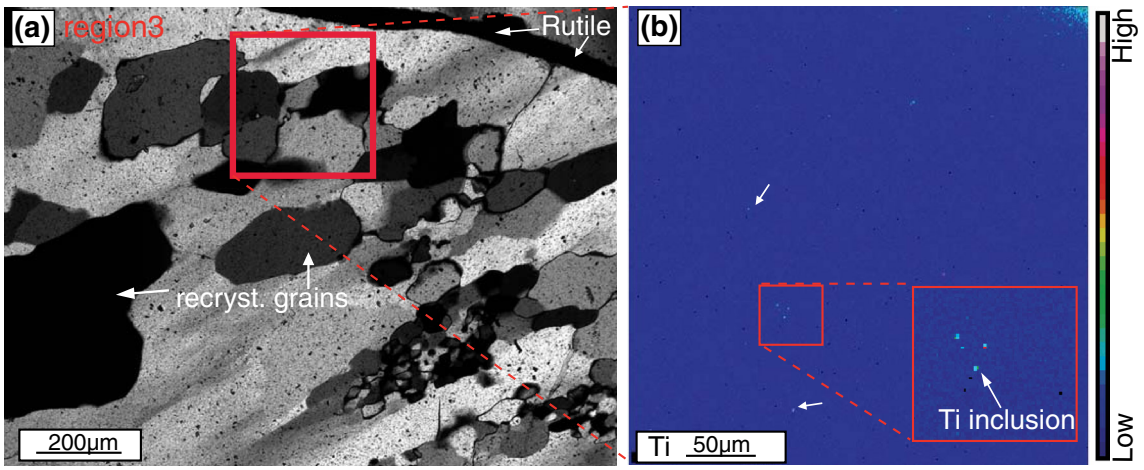

Fig. 6 Ti-distribution in the recrystallized region 3 of sample mn319. **a** Cross-polarized light micrograph of the recrystallized zone. Estimated deformation temperature: 890 °C. The red square indicates the position, where the element distribution map was acquired (see part **b**). Note the large (up to 300 µm) recrystallized grains with lobate grain boundaries and irregular grain shape typical for grain boundary migration recrystallization (GBM) induced by static recrystallization. **b** Element distribution map of the region with recrystallized grains and original undeformed single crystal. *Arrows* indicate small Ti inclusions distributed along grain boundaries and in grain triple junctions. The *inset* shows a detail of small Ti inclusions. The *upper right corner* of the map show a higher Ti content produced by analytical artifacts caused by the presence of rutile along the sample boundary

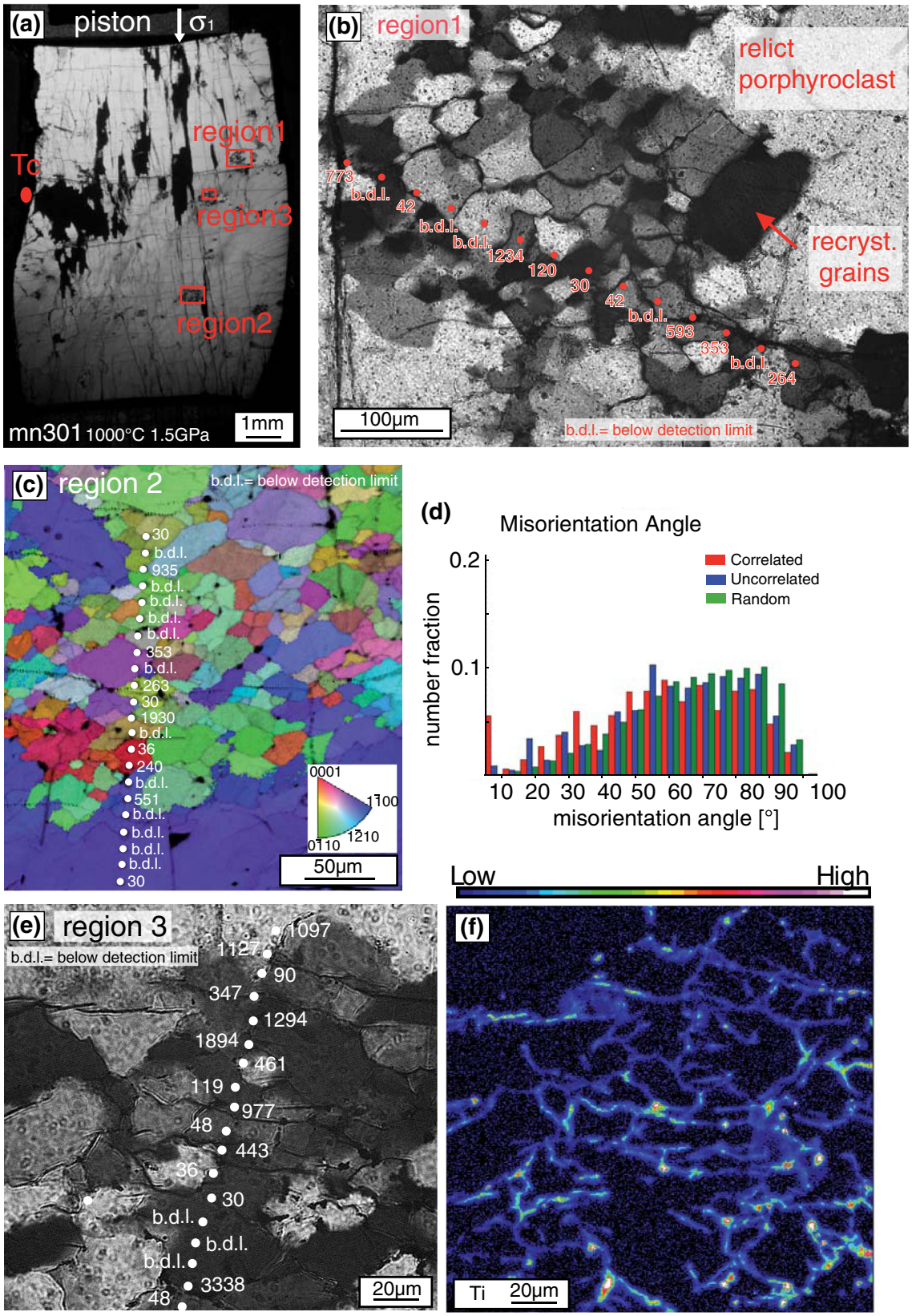
(a)
piston
σ1
Tc
region1
region3
region2
mn301 1000°C 1.5GPa
1mm
(b)
region1
relict porphyroclast
773
b.d.l.
42
b.d.l.
b.d.l.
1234
120
30
42
b.d.l.
593
353
b.d.l.
264
recryst. grains
100µm
b.d.l.= below detection limit
(c)
region 2
b.d.l.= below detection limit
30
b.d.l.
935
b.d.l.
b.d.l.
b.d.l.
b.d.l.
353
b.d.l.
263
30
1930
b.d.l.
36
240
b.d.l.
551
b.d.l.
b.d.l.
b.d.l.
b.d.l.
30
0001
1100
0110
1210
50µm
(d)
Misorientation Angle
Correlated
Uncorrelated
Random
number fraction
0.2
0.1
10 20 30 40 50 60 70 80 90 100
misorientation angle [°]
Low
High
(e)
region 3
b.d.l.= below detection limit
1097
1127
90
347
1294
1894
461
119
977
48
443
36
30
b.d.l.
b.d.l.
b.d.l.
3338
48
20µm
(f)
Ti 20µm

◀**Fig. 7** Microstructures and chemical composition of sample mn301 deformed at 1,000 °C, 1.5 GPa in the presence of TiO_2 powder and fluid (H_2O). Experimental shortening direction is *vertical* in all images. **a** Cross-polarized light micrograph of sample mn301. Final position of the thermocouple (Tc) and position of the analyzed regions are marked in *red*. *Longitudinal cracks* are visible as a consequence of hitting the sample at low confining pressure and temperature prior deformation. *Horizontal cracks* developed during quenching and unloading of the sample after deformation. Crystal–plastic deformation is localized in distributed pockets of recrystallized quartz grains (*red boxes*). **b** Light micrograph (cross-polarized) image of a recrystallized pocket (region 1), local temperature 981 °C. In red are marked the Ti (ppm) content measured by EMPA. Expected equilibrium content at these conditions is 226 ppm Ti. Note the large variation of Ti content in the zone: the central parts of the recrystallized grains show uniformly low contents (below detection limit to 42 ppm), whereas grain boundaries can show extremely high Ti contents (264–1,234 ppm). **c** EBSD Orientation map of region 2. The crystallographic orientations in the map are color-coded according to the inverse pole figure given in the *lower corner* of the image. Indicated in *white* are the Ti contents (ppm) measured with the microprobe (detection limit 20 ppm). Grain boundaries and grains triple junctions show high Ti contents, whereas the central parts of the recrystallized grains and the undeformed quartz (lower part, in *blue*) show Ti contents much lower than the expected equilibrium value of 186 ppm. **d** Frequency distribution of misorientation angle between nearest neighbor pixels (correlated, *red bars*) and for any pairs in the data set (uncorrelated, *blue bars*). For reference, the distribution of a data set with random orientation (*green bars*) is given. **e** Light micrograph of recrystallized region 3 with measured Ti contents (in ppm). **(f)** Element distribution map acquired by EPMA. Rutile grains (*red* to *light blue color*) are present along grain boundaries and triple junctions, indicating mobility of TiO_2 during the experiment

relicts display undulatory extinction, a high density of low angle misorientations, and incipient subgrain formation at their boundaries (red in Fig. 9a). The subgrains have an estimated mean size of ~10 to 25 μm. The recrystallized bands consist of grains with irregular grain shapes and with a grain size varying from ~5 to 65 μm (mean size of ~25 μm; Figs. 8b, 9c). Locally, some single grains can reach diameters of up to 150 μm (Fig. 8b). Grains have lobate boundaries, and pinning structures are also present (Fig. 8b). Some recrystallized grains show internal deformation and subgrain boundaries (marked in red in Fig. 9a). The misorientation angle distribution (Fig. 9b) shows an elevated frequency of low angle misorientations <15°, but these are less frequent than in lower temperature samples. On the other hand, high misorientation angles (50°–90°) are much more frequent than in samples deformed at lower temperatures but less frequent than random (Fig. 9b).

EMPA analysis on two recrystallized regions deformed at 978 °C (region 1, Fig. 8b) and 1,000 °C (region 2, Fig. 9b) shows in both cases a strong variation in the Ti content: A majority of the spot analyses result in Ti contents close to the detection limit of the microprobe (20 ppm), whereas a few analyses show values of several hundred ppm Ti (Fig. 8b). Ti contents below and close to the detection limit are measured in the internal parts of the recrystallized grains, whereas high Ti contents (78–233 ppm) are found at grain boundaries and grain triple junctions (Fig. 8b).

Sample mn332 (Fig. 8c, d) was deformed for 120 h and then annealed at hydrostatic conditions (1,000 °C and 1.5 GPa) for 139 h. Even though recrystallization is distributed throughout the sample, deformation is not uniformly accommodated: Recrystallization occurs in discrete bands that have an orientation approximately parallel to the loading direction (σ_1). Many bands appear in a crack-like distribution, especially in the lower, less recrystallized, part of the sample (Fig. 8c). Between the recrystallized bands, lesser deformed relict crystal material is present (Fig. 8c, d). The recrystallized quartz shows variable grain size: The grains in the relatively rutile-free areas are up to 150 μm in width, whereas those within rutile-rich areas are smaller (15 μm) (Fig. 8d). Where rutile needles are present at the grain boundaries, the grains show evidence of pinning structures (Fig. 8b, d). EMPA measurements on sample mn332 were carefully taken only in the central parts of recrystallized grains; all values are below the detection limit of the instrument (Fig. 8d).

Sample mn331 (Fig. 8e, f) was first deformed with a strain rate of 10^{-6} s^{-1} up to peak strength and afterward was deformed for 244 h with a strain rate of 10^{-7} s^{-1}. In the heterogeneously deformed sample, strain was accommodated principally in the central part of the sample (the upper part was lost during sample preparation; Fig. 8e), whereas the lower and edge regions display only weak deformation characterized by undulose and patchy extinction. The crack-like distribution of the recrystallized bands is even more pronounced than in sample mn332, especially in the lower part of the sample (Fig. 8e). The recrystallized quartz bands often consist of diamond-shaped grains with sizes varying from 15 to 180 μm (Fig. 8e) and with weakly lobate grain boundaries (Fig. 8f). EMPA analyses of the internal parts of newly recrystallized grains reveal Ti contents below the detection limit of the instrument (Fig. 8f). Further, no Ti variation was observed between undeformed host quartz grains and recrystallized new grains (Fig. 8f).

In samples deformed at 1,000 °C, there appears to be a succession of progressively evolving microstructures from low strain samples, in which recrystallized bands have a crack-like distribution (Fig. 8e; sample mn331), to high strain samples, in which the recrystallized bands accommodate most of the bulk strain (Fig. 8a; sample mn326). In all samples, however, the recrystallized grain shapes are similar (Fig. 8).

Discussion

Mechanical data

Strength differences between 0^+ and ⊥m orientations at 900 and 1,000 °C (Fig. 3) are not systematic and most

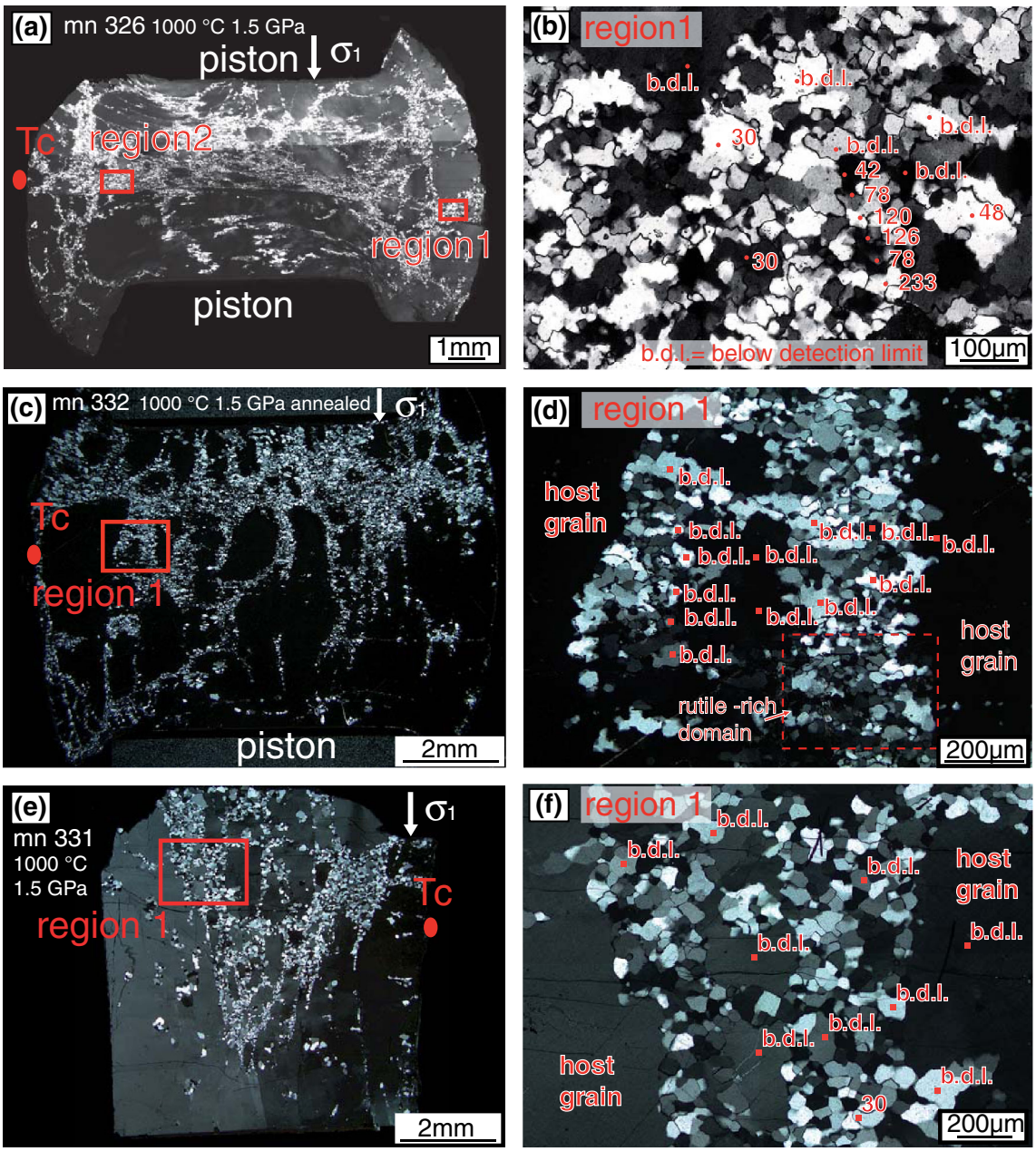

Fig. 8 Recrystallized microstructures and chemical composition of a quartz single crystals deformed with the addition of TiO_2 powder and fluid (H_2O) at 1,000 °C, 1.5 GPa. All images are cross-polarized light micrographs. Compression direction is *vertical* in all images. Final position of the thermocouple (Tc) and position of the analyzed regions are marked in *red* **a**, **b** sample mn326 deformed at a strain rate of 10^{-6} s^{-1} for 93 h. **c**, **d** sample mn332 deformed at a strain rate of 10^{-6} s^{-1} for 120 h and annealed afterward for 139 h at the same conditions. **e**, **f** sample mn331 deformed at a strain rate of 10^{-7} s^{-1} for 244 h. All samples show the typical high temperature recrystallization microstructures. Note the strongly irregular grain shape, the variable grain size and the lobate grain boundaries with local pinning structures typical for recrystallization by grain boundary migration (GBMR) in the samples mn326 and mn332. Note the small grain size of the recrystallized quartz grains in the rutile-rich domain of sample mn332. Sample mn331 shows variable grain size and quite straight grain boundaries. The Ti contents in ppm, marked in red, show the same trend as in sample mn301 with high Ti content at grain boundaries and low contents in the central part of the recrystallized grains

likely due to strain partitioning, which is a general feature of many natural single-crystal experiments (e.g., Griggs and Blacic 1964, Vernooij et al. 2006a, b). Localization of recrystallization is common and leads to strain partitioning. The experiments on natural "wet" single crystals carried out in this study under controlled crystal orientation, pressure, temperature and strain rate conditions only show approximately reproducible mechanical behavior (Fig. 3).

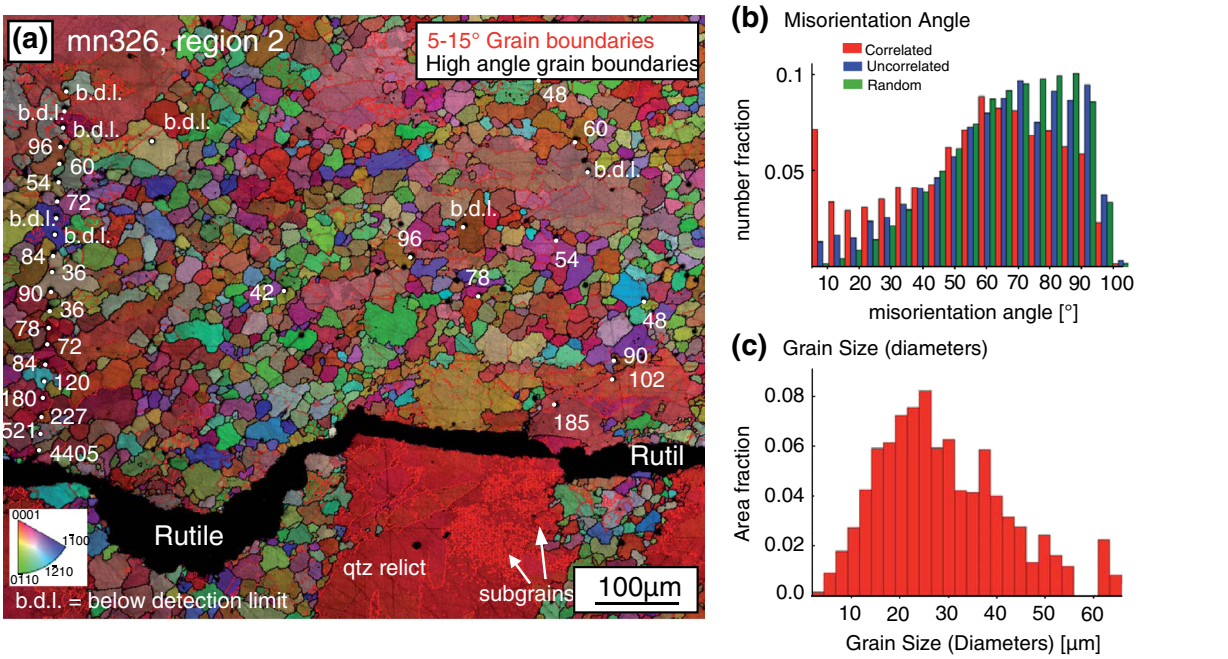

Fig. 9 EBSD results of sample mn326 deformed at 1,000 °C, 1.5 GPa. **a** EBSD Orientation map of region 2. The crystallographic orientations are color-coded according to the inverse pole figure given in the *lower corner* of the image. *Black lines* represent grain boundaries with misorientation angles >15°, *red lines* misorientation angles <15°. Ti contents (ppm) are marked by *white numbers*. Note the high Ti contents close to the rutile (in *crack*) caused by phantom Ti in Quartz. Small (~10 to 25 µm) subgrains are visible within and at the boundaries of quartz relicts. **b** Frequency distribution of misorientation angles between nearest neighbor pixels (correlated, *red bars*, uncorrelated pairs, *blue bars*, random orientation, *green bars*). **c** Grain size distribution (area fraction) of recrystallized region 2. The grain size of the recrystallized grains varies from a few µm up to 65 µm, but the mean grain size is on the order of 20–25 µm

The direct comparison of single crystals versus polycrystalline material experiments is difficult, because in single crystals, the onset of recrystallization requires higher strain, and strain partitioning is more pronounced. However, a qualitative comparison of the mechanical behavior of the two starting materials (single crystals versus polycrystalline material) is possible.

In our series of experiments, samples deformed at 800 and 900 °C show high peak strengths followed by pronounced weakening, whereas at 1,000 °C, samples deform by more steady state flow at lower stresses (flow stresses of ~80 to 250 MPa; Fig. 3). In the experiments of Hirth and Tullis (1992), the same pronounced weakening after peak strength is observed in polycrystalline Heavitree quartzite deformed in "regime 1," where the recrystallization takes place by bulging recrystallization, but at lower temperatures (700 °C). In our experiments, the recrystallization mechanism is somewhat different for the same type of mechanical behavior (see section below).

Hirth and Tullis (1992) observed steady state flow in samples deformed at 800 °C and higher (regime 2 and 3), where deformation was accompanied by rotation recrystallization (progressive subgrain rotation, SGR) and GBMR. Comparison of our mechanical data with those of Hirth and Tullis (1992, for as is samples) indicates that our experiments show generally similar mechanical behavior, but at flow stresses, which are 100–300 MPa higher at the same temperatures and strain rates. The data by Stipp et al. (2006), who performed water-added experiments as in our case, show 50 MPa lower flow stress in 1,000 °C experiments, 40–140 MPa lower in 900 °C experiments and 230 MPa lower in 800 °C experiments at similar strain rates as in our experiments (comparing end strengths at the highest volume of recrystallized grains in our samples).

The differences in flow stress between polycrystalline and single-crystal experiments most likely arise from the inhomogeneous distribution of strain within the single-crystal samples. The strain partitioning coincides with the location of regions of recrystallization (e.g., Figs. 4, 5, 8) and the distribution and content of H_2O (in the form of fluid inclusions). Although we carefully chose homogeneous milky regions of the quartz single crystal, the local distribution of fluid inclusions varies within a sample and causes strain partitioning. Nevertheless, the experiments show a general trend of decreasing flow stress with increasing temperature and, together with the dynamic recrystallization microstructures, indicate the activation of dislocation creep deformation.

Microstructures

The dynamic recrystallization mechanisms are expected to be important for the exchange of Ti in quartz (Grujic et al. 2011; Härtel and Herweg 2013). Therefore, one of the main tasks of this study was to test the potential effect of different recrystallization mechanisms on Ti exchange. Below, the recrystallization mechanisms in the experiments are first discussed and then related to the measured Ti content of the new quartz grains.

Dynamic recrystallization commonly occurs by the transformation and/or movement of grain boundaries through the crystal. In polycrystalline rocks, grain boundaries are already present in the starting material, whereas in single crystals, they first need to be formed. As demonstrated by Vernooij et al. (2006a, b), the initial stage of recrystallization in a quartz single crystal may occur by the formation of microfractures. Along those microcracks, small fragments and local crystal misorientations are formed. With increasing strain, these fragments and the small misoriented crystal domains grow and form recrystallized grains that undergo crystal plastic deformation. The same features have been observed by Stünitz et al. (2003) in feldspar single crystals.

In our lower strain samples, initiation and localization of deformation in longitudinal narrow bands oriented parallel to the σ_1 direction are evident (Fig. 8e). With increasing strain (Fig. 8a, c), the recrystallized bands widen and become locally displaced. The specific dynamic recrystallization mechanism operating in the bands is temperature, strain rate, water content and grain size dependent (e.g., Hirth and Tullis 1992; Stipp et al. 2002a, b, 2006, 2010). As the experiments reported here were performed over a relatively wide range of pressure and temperature conditions, different recrystallization mechanisms are activated during deformation.

At 800 °C, recrystallization occurred predominantly by SGR (e.g., Guillope and Poirier 1979; White 1976; Urai et al. 1986; Wheeler et al. 2001), suggested by the formation of core and mantle structures, the high frequency of low angle misorientations (Fig. 4) and the grain size distribution of subgrains and recrystallized grains. With increasing temperature (900 °C), the recrystallized quartz shows evidence for recrystallization accommodated by a combination of SGR and GBM (e.g., irregular grain shapes, lobate and partly straight grain boundaries, local pinning; Gottstein and Mecking 1985; Urai et al. 1986; Jessell 1987). It is likely that a large part of the GBM occurred during the annealing stage of the experiment, but some of the migration may have started in relatively low strain rate domains as deformation was partitioned within the sample. At high temperatures (1,000 °C), recrystallization still occured by a combination of SGR and GBM; however, at this temperature, the GBM microstructures represent dynamic recrystallization, because the deformed quartz samples were quenched immediately after deformation.

The equilibrium grain size of dynamically recrystallized rock (during steady state flow) is dependent on the applied stress (e.g., Derby 1991). Considering the stable flow stress of c. 80 MPa reached by sample mn326, the equilibrium recrystallized grain size predicted by the quartz piezometer of Stipp and Tullis (2003) at our experimental conditions would be $\sim$15 μm. The size of the subgrains observed within and around the porphyroclasts in the central part of the sample is $\sim$10 to 25 μm (Fig. 9), corresponding to a flow stress of 30–80 MPa (Stipp and Tullis 2003), and suggesting that the original size of newly recrystallized grains in this sample was similar to that predicted by the quartz piezometer. However, large recrystallized grains with diameters up to 150 μm are present in the peripheral regions of the sample. As discussed above (for the recrystallization bands), with increasing strain, partitioning parts of the sample may cease to deform (e.g., close to the alumina pistons). In this situation, grain growth is favored over dynamic recrystallization. The local abnormal grain growth in sample mn326 is interpreted as a result of annealing of parts of the samples during strain partitioning.

According to Stipp et al. (2010), the highest temperature/lowest strain rate conditions attainable in deformation experiments yield microstructures in a transition region between GBM and SGR mechanisms (between regime 2 and 3). In our samples, however, there is ample evidence for dominant boundary migration microstructures (i.e., regime 3). We suggest that the most important reason for this difference is the strain partitioning and partial annealing discussed above.

Relationship between deformation and Ti re-equilibration in quartz

The amount of Ti that can be incorporated into a quartz crystal depends on temperature (Ostapenko et al. 2007; Wark and Watson 2006), pressure (Ostapenko et al. 2007; Thomas et al. 2010) and the growth rate of the crystals (Huang and Audétat 2012). Based on the data of Thomas et al. (2010) and the fact that TitaniQ can be applied to deformed and metamorphic rocks as suggested by Kohn and Northrup (2009), we would expect recrystallized grains in our deformed quartz samples to have Ti values ranging from 117 to 256 ppm (see Table 3). However, the recrystallized grains of the deformed samples show much lower Ti contents, mostly below the detection limit (20 ppm) of the electron microprobe.

In samples deformed at 800 °C, EPMA analysis on the undeformed regions, along bands of undulatory extinction, and in zones with core and mantle structures, shows no Ti

Table 3 Calculated and measured Ti contents in the deformed quartz single crystal

Sample	Exp. T (°C)	Region	T (°C) deviation	Calculated T (°C)	Expected Ti (ppm)	Measured Ti (ppm) (repr. value)
mn277	800	2	0	800	147	b.d.l.
mn319	900	1	−6	894	121	b.d.l.
		2	0	900	127	b.d.l.
mn301	1,000	1	−19	981	226	b.d.l.
		2	−47	953	186	b.d.l.
		3	0	1,000	256	b.d.l.
mn326	1,000	1	−22	978	222	30
		2	0	1,000	256	36
mn331	1,000	1	0	1,000	256	b.d.l.
mn332	1,000	1	0	1,000	256	b.d.l.

Calculation of the expected equilibrium Ti content in the analyzed zones, considering the temperature deviation caused by the temperature gradient (=temperature decrease of around 10 % from the center of the sample to its end). Expected Ti contents were calculated as: RT ln $X_{TiO2}^{quartz} = -60{,}952 + 1.520 * T(K) - 1{,}741 * p$ (kbar) + RT ln a TiO_2 (Thomas et al. 2010), where a TiO_2 was 1 since rutile is present in all samples, $R = 8.3145$ J/K (gas constant), T is temperature in °K and p is confining pressure in kbar. The conversion from TiO_2 to Ti (ppm) occurred according to the formula of Thomas et al. (2010). The representative value for the measured contents was calculated as the average of the measurements, which were taken at a minimal distance of 100 μm from the rutile inclusions, in order to avoid errors caused by phantom Ti in quartz. Note that all the representative values are close or below the detection limit (b.d.l.) of the instrument

exchange. All measurements of Ti were below the detection limit (20 ppm) of the instrument. Also in the experiments at 900 °C, the Ti values were uniformly low across the whole sample. Element distribution maps and point analyses reveal no Ti enrichment in the small, recrystallized grains or in large grains, which underwent grain growth.

In experiments performed at 1,000 °C, very high Ti values locally alternate with values below the detection limit. Element distribution maps indicate no Ti re-equilibration in the internal parts of the recrystallized grains and high Ti contents along grain boundaries, caused by the presence of small rutile needles which crystallized in dilatant sites or by small rutile inclusions distributed along the grain boundaries. The presence of precipitated Ti-phases along grain boundaries generates secondary analytical artifacts, leading to apparently high Ti contents in the border regions of adjacent quartz grains. However, point analyses of grains deformed at 1,000 °C indicate uniformly low Ti contents (below the detection limit) in the interior parts of the recrystallized grains. We conclude that the Si–Ti substitution in quartz, the basis for the TitaniQ geothermobarometer (Ostapenko et al. 2007; Wark and Watson 2006), does not occur in our experimentally deformed quartz single crystals under the deformation conditions investigated here.

Possible factors that may inhibit Ti re-equilibration during these experiments are as follows:

(1) No Ti was available at the sites of exchange due to limited mobility of Ti during the experiments. (2) The kinetics of the exchange processes are too slow in the experiments (for example a slow growth rate of recrystallizing grains). (3) The recrystallization mechanisms do not allow ionic exchange during the experiments. (4) The activation energy for the atomic substitution is too high in the solid state, and complete reconstitution by solution precipitation has not been achieved in the experiments. Below, we discuss each of these possibilities individually.

1. Fine-grained TiO_2 powder (0.2 g) was placed around the quartz single crystal or between individual pieces of single crystals in a welded jacket prior to deformation. After deformation, we observed large aggregates of euhedral rutile inside deformed quartz grains. Rutile precipitates occur on grain boundaries of recrystallized quartz grains and along cracks (Fig. 2). The nucleation and growth of rutile in these sites indicate that Ti was available at the locations of recrystallization (=moving grain boundaries) and that essentially all new quartz grains recrystallized under rutile saturated conditions. Ti was most likely transported in the sample through fluids along grain boundaries during the deformation process. Due to the presence of rutile in all samples, we assume a TiO_2 activity of =1 (see also Thomas et al. 2010).
2. The kinetics and growth rate of crystals have an influence on the amount of trace elements that can be incorporated in the crystal. Huang and Audétat (2011) propose an increase in Ti concentration with increasing growth rate of newly formed quartz. This arises from the fact that trace element incorporation is aided by imperfect crystal growth, which is more likely to occur in crystals that are relatively fast grown (e.g., Martin and Armington 1983) and/or by the fact that in fast-

grown crystals, diffusional reorganization of the crystal lattice is limited (Watson and Liang 1995; Watson 2004). In domain II of sample mn319, the newly recrystallized grains formed by subgrain rotation have a size of 2–10 μm (Fig. 5). During deformation and annealing, the quartz grains grew up to 500 μm due to the mobility of some grain boundaries (abnormal grain growth). At a run time of 5 days (time calculated after reaching peak strength, which should coincide with the onset of recrystallization, Hirth and Tullis 1992) and considering an initial grain size of 2–10 μm and a concentric growth of the grains, this translates to a growth rate varying from <1 to 50 μm day^{-1} (Table 4). A growth rate difference of around 50 μm day^{-1} led in the experiments of Huang and Audétat (2012) to Ti variations of around 80 ppm. However, in our experiments, large grains and small grains (which grew at different growth rates) show no systematic difference in Ti content and in both cases, the Ti values are much lower than expected. We conclude that the growth rates of the new grains formed by recrystallization and the growth rate variation are not responsible for the lack of Ti exchange in the deformed samples.

3. At temperatures of 800 and 900 °C in our experiments, deformation occurred mainly by subgrain rotation recrystallization (SGR). During SGR, new grains develop by progressive misorientation of the crystal lattice, but the new grains inherit the internal structure and defects of the old grains. During this process, new grain boundaries form by volume diffusion processes inside the old quartz grains without interacting with a fluid. In this case, no re-equilibration of Ti is expected, which is in agreement with our measurements and observations. At higher temperatures (1,000 °C), recrystallization of quartz occurred by a combination of SGR and GBM (i.e., local displacement of the grain boundaries; Gottstein and Mecking 1985; Guillope and Poirier 1979). The migration of grain boundaries (regardless of whether this occurs as SIGM, CIGM, or by grain growth) involves the transfer of material and ionic exchange is expected. Rapid chemical changes in the solid material produced by migration of boundaries and related ionic exchange have been documented in experiments conducted on carbonate bicrystals by Evans et al. (1986) and Hay and Evans (1987a, b). Our boundary migration velocities (Log V_{mig} in microns h^{-1}) are similar to those of Hay and Evans (1987a), even though the homologous temperature in our experiments is lower (T/T_m = 0.4–0.5) and is in the range of that of many of the tested metal and ceramic systems cited in Hay and Evans (1987a) and by Huang and Audétat (2012). Substantial changes in composition in the wake of moving boundaries have been recorded in carbonates by Hay and Evans (1987a, b). In our experiments, both GBM and grain growth occurred by migrating Ti-saturated boundary zones, probably wetted by a fluid film. Therefore, solute exchange of Ti between the recrystallized quartz grains and the Ti-saturated fluid is expected at much faster rates than by volume Ti diffusion in quartz. However, there was incomplete or no Ti exchange in the grains deformed by GBM. We conclude that Ti was not incorporated (or only at levels far below the equilibrium concentration) into the crystal structure despite extensive structure reconstitution during recrystallization by boundary migration and grain growth, and ideal conditions for rapid ionic exchange (presence of Ti-saturated fluid, mobility of grain boundaries, reconstitution of the crystal structure).

4. Atomic substitution of Si by Ti is demonstrated in the studies of Wark and Watson (2006), Thomas et al. (2010), Huang and Audétat (2012) where the synthetic quartz crystals were crystallized and rapidly grown from amorphous SiO_2 in rutile-bearing H_2O fluid. Likewise, during crystallization from a melt, substituting elements are easily incorporated into the quartz structure as observed by Rankama and Sahama (1950) and Jacamon and Larsen (2009). Conversely, once the quartz crystals have formed with low Ti contents, Si has to be exchanged for Ti to adjust the composition to the new equilibrium composition, e.g., at changing P,T conditions. As predicted by Ostapenko et al. (2007) and Wark and Watson (2006), the incorporation of Ti into quartz occurs by a simple substitution, where a tetravalent Ti atom is substituted with a tetravalent Si atom. Atomic substitutions in crystalline materials occur when the valences of substituting ions are similar (difference not greater than = 1) and when the substituting ions have a similar size (size difference <15 %). The ionic radius of Si^{4+} (0.40 Å) is almost 40 % smaller than that of Ti^{4+} (0.61 Å) (Perkins 2002). Furthermore, the Si–O bond is a very strong covalent bond (Flem et al. 2002), so that the energy required for the solid-state substitution of Si by Ti is high. Therefore, it is conceivable that substitution of Si by Ti only takes place by complete dissolution of the quartz and precipitation from a fluid-rich aqueous environment, where Ti-transport is very fast. For example, Larsen et al. (2004) observed the immobility of Ti during recrystallization of igneous quartz.

Table 4 Grain size and growth rate of the recrystallized quartz grains. The grain size (diameter) is defined by the major diameter of an ellipse having the same area as the grains. Growth rate (μm day^{-1}) calculated as grain size (radius) divided by the experimental time after reaching peak strength (onset of recrystallization)

Sample	T (°C) experiment		Grain size (diameter) (μm)	Time after peak strength (days)	Growth rate (μm day^{-1})
mn319	900	Region 2	6–100	5	<1–10
		Region 3	30–500	5	3–50
mn301	1,000	Region 1	10–150	3	1–25
		Region 2	10–80	3	1–13
mn326	1,000	Region 1	10–150	4	1–19
		Region 2	10–65	4	1–8
mn331	1,000	Region 1	15–180	10	<1–9
mn332	1,000	Region 1	15–150	10	<1–7

Incorporation of Ti-atoms into the quartz lattice during dynamic recrystallization could be insufficient because of sluggish Ti-transport and because of incomplete reconstitution processes of the quartz crystal structure during GBM. Hay and Evans (1987a, b) and Evans et al. (1986) observed progressive chemical changes behind repeated oscillatory grain boundary movement in carbonates. Thus, it may be necessary to move grain boundaries repeatedly through a crystal structure to achieve an equilibrium composition by CIGM. Some of the more elevated Ti contents of recrystallized grains in our experiments may indicate limited Ti exchange (Figs. 7, 9), but the values are much lower than the expected equilibrium contents. The total strain for SIGM, the free energy difference for CIGM and SIGM, and the repeated number of migration cycles required to reach equilibrium Ti contents may well exceed the conditions of our experiments.

Applicability of the TitaniQ geothermometer to deformed rocks

Kohn and Northrup (2009) suggested that TitaniQ accurately determines dynamic recrystallization temperatures and therefore can be applied to quartz-bearing mylonites. However, our experiments demonstrate that Ti is not incorporated into the crystal structure during recrystallization, even in a fluid-bearing and Ti-saturated environment at the investigated deformation conditions (T = 800–1,000 °C, P = 1–1.5 GPa, strain rates 10^{-6}–10^{-7} s^{-1}, total strains of up to 47 %), regardless of the specific recrystallization mechanism. This raises questions as to the applicability of the TitaniQ geothermobarometer to prograde metamorphic rocks, which experienced deformation and recrystallization.

Conversely, during retrograde deformation, the decrease in temperature and/or pressure may favor the removal, by exsolution or diffusion, of the Ti-atoms from the quartz structure. The removal process is energetically and kinetically favored over the incorporation process due to the fact that the Ti-atoms in the quartz crystal structure act as a defect (larger size, see above). The removal of Ti from the crystal lattice causes precipitation and accumulation of Ti-phases along the grain boundaries. As shown here, measurements on fine-grained recrystallized regions where rutile is present at grain boundaries can lead to erroneous results due to analytical artifacts caused by phantom Ti (EMPA measurements) or poor spatial resolution (large spot size of SIMS, LA-ICPMS). The problem of measuring the real Ti content in fine-grained aggregates could explain the conflicting results obtained by applying the TitaniQ to naturally deformed rocks (e.g., Grujic et al. 2011; Wilson et al. 2012). We conclude that the application of the TitaniQ geothermobarometer to deformed metamorphic rocks at low fluid contents may not be as straightforward as previously thought, at least under prograde metamorphic conditions where low Ti contents have to be adjusted to higher equilibrium contents. In retrograde conditions, Ti exchange may be easier but may present analytical problems with exsolved Ti at grain boundaries, especially at small grain sizes resulting from the higher stresses of deformation. The problem of Ti incorporation and attainment of equilibrium in deforming quartz requires further research.

Conclusions

Our experiments demonstrate that in a fluid-present and Ti-saturated environment, the isomorphic Si–Ti substitution in quartz is not likely to occur during deformation, regardless of the recrystallization mechanism involved in the deformation process. In our experiments, equilibrated Ti contents were neither found in quartz grains formed by subgrain rotation recrystallization nor in those showing evident GBM features (lobate grain boundaries, pinning, grain growth). Instead, the Ti contents are similar to that of the original, undeformed quartz single crystal. Where Ti contents are higher, they never reach the equilibrium concentrations expected for the given T–P conditions. The TitaniQ geothermobarometer has been demonstrated to

accurately determine *P–T* conditions of quartz crystallization from a melt or hydrothermal fluid (Rusk et al. 2008; Barker et al. 2010). However, Si–Ti exchange appears to be inhibited, or to take place by different mechanisms, in experimentally deformed quartz crystals. One major difference between the experiments reported here and those used to calibrate the TitaniQ geothermobarometer (deformation and hydrostatic piston cylinder experiments; Wark and Watson 2006; Hayden and Watson 2007; Thomas et al. 2010; Huang and Audétat 2012) is our use of considerably lower H_2O-contents. The lower H_2O-contents most likely correspond more to those in natural metamorphic and deformation settings. Due to the limited or inhibited exchange of Ti during dynamic recrystallization of quartz at low concentrations of H_2O, care should be taken when applying the TitaniQ geothermobarometer to deformed rocks under prograde metamorphic conditions. Si–Ti exchange in quartz crystals and Ti-equilibration is more likely to occur during retrograde conditions in recrystallized quartz, because Ti is to be exsolved and/or removed by diffusion. The exchange mechanisms of exsolution under such conditions may be kinetically more favorable. It remains uncertain whether TitaniQ can be applied to determine the *P–T* conditions of migmatite in which partial melting occurs or to lower temperature prograde rocks (e.g., Storm and Spears 2009; Spear and Wark 2009, Grujic et al. 2011; Menegon et al. 2011).

References

Adachi T, Hokada T, Osanai Y, Toyoshima T, Baba S, Nakano N (2010) Titanium behavior in quartz during retrograde hydration: occurrence of rutile exsolution and implications for metamorphic processes in the Sør Rondane Mountains, East Antarctica. Polar Sci 3:222–234. doi:10.1016/j.polar.2009.08.005

Adams BL, Wright SI, Kunze K (1993) Orientation imaging: the emergence of a new microscopy. Metall Trans A 24:819–831

Baeta RD, Ashbee KH (1969a) Slip system in quartz: I experiments. Am Mineral 54:1551–1573

Baeta RD, Ashbee KH (1969b) Slip system in quartz: II interpretation. Am Mineral 54:1574–1582

Barker AK, Coogan LA, Gillis KM, Hayman NW, Weis D (2010) Direct observation of a fossil high-temperature, fault-hosted, hydrothermal upflow zone in crust formed at the East Pacific Rise. Geology 38:379–382. doi:10.1130/G30542.1

Bastin GF, Van Loo FJJ, Vosters PJC, Vrolijk JWGA (1984) An iterative procedure for the correction of secondary fluorescence effects in electron-probe microanalysis near phase boundaries. Spectrochim Acta B 39:1517–1522. doi:10.1016/0584-8547(84)80174-3

Blacic JD, Christie JM (1984) Plasticity and hydrolytic weakening of quartz single crystals. J Geophys Res 89:4223–4239

Campbell ME, Hanson JB, Minarik WG, Stix J (2009) Thermal history of the bandelier magmatic system: evidence for magmatic injection and recharge at 1.61 Ma as revealed by cathodoluminescence and titanium geothermometry. J Geol 117:469–485. doi:10.1086/604744

Cherniak DJ, Watson BE, Wark DA (2007) Ti diffusion in quartz. Chem Geol 236:65–74. doi:10.1016/j.chemgeo.2006.09.001

Derby B (1991) The dependence of grain size on stress during dynamic recrystallization. Acta Metall 39:955–962

Donovan JJ, Lowers HA, Rusk BG (2011) Improved electron probe microanalysis of trace elements in quartz. Am Mineral 96:274–282. doi:10.2138/am2011.3631

Drury MR, Urai JL (1990) Deformation-related recrystallization processes. Tectonophysics 172:235–253

Evans B, Hay RS, Shimizu N (1986) Diffusion-induced grain-boundary migration in calcite. Geology 14:60–63. doi:10.1130/0091-7613(1986)14<60

Flem B, Larsen RB, Grimstvedt A, Mansfeld J (2002) In situ analysis of trace elements in quartz by using laser ablation inductively coupled plasma mass spectrometry. Chem Geol 182:237–247. doi:10.1016/S0009-2541(01)00292-3

Fournelle J (2007) Problems in trace elements EMPA: modeling secondary fluorescence with PENEPMA. EOS transactions American Geophysical Union 88:52. Abstract V51A-0329

Frondel C (1962) Silica Minerals. In: Dana JD, Dana ES (eds) The system of mineralogy. Wiley, New York

Fynn GW, Powell WJA (1979) The cutting and polishing of electro-optical minerals. Adams Higer, London, p 216

Girard G, Stix J (2010) Rapid extraction of discrete magma batches from a large differentiating magma chamber: the Central Plateau Member rhyolites, Yellowstone Caldera, Wyoming. Contrib Miner Petrol 160:441–465. doi:10.1007/s00410-009-0487-1

Gottstein G, Mecking H (1985) Recrystallization. In: Wenk HR (ed) Preferred orientation in deformed metals and rocks: an introduction to modern texture analysis. Academic Press, Orlando, pp 183–218

Griggs D, Blacic JD (1964) The strength of quartz in the ductile regime. Transactions American Geophysical Union 45:102–103

Griggs D (1967) Hydrolytic weakening of quartz and other silicates. Geophys J Roy Astron Soc 14:19–31

Grujic D, Stipp M, Wooden JL (2011) Thermometry of quartz mylonites: importance of dynamic recrystallization on Ti-in-quartz reequilibration. Geochem Geophys Geosyst 12:1–19. doi:10.1029/2010GC003368

Guillope M, Poirier JP (1979) Dynamic recrystallization during creep of single-crystalline halite: an experimental study. J Geophys Res 84:5557–5567

Härtel M, Herweg M (2013) Titanium-in-quartz thermometry on synkinematic quartz veins in a retrograde crustal-scale normal fault zone. Tectonophysics 608:468–481

Hay RS, Evans B (1987a) Chemically induced migration in low and high angle calcite grain boundaries. Acta Metall 35:2049–2062

Hay RS, Evans B (1987b) Chemically induced grain boundary migration in calcite: temperature dependence, phenomenology, and possible applications to geologic systems. Contrib Miner Petrol 97:127–141

Hayden LA, Watson BE (2007) Rutile saturation in hydrous siliceous melts and its bearing on Ti-thermometry of quartz and zircon. Earth Planet Sci Lett 258:561–568. doi:10.1016/j.epsl.2007.04.020

Hermann J, O'Neill HSC, Berry AJ (2005) Titanium solubility in olivine in the system TiO_2–MgO–SiO_2: no evidence for an ultra-deep origin of Ti-bearing olivine. Contrib Miner Petrol 148:746–760. doi:10.1007/s00410-004-0637-4

Hirth G, Tullis J (1992) Dislocation creep regimes in quartz aggregates. J Struct Geol 14:145–159. doi:10.1016/0191-8141(92)90053-Y

Hirth G, Teyssier C, Dunlap J (2001) An evaluation of quartzite flow laws based on comparisons between experimentally and

naturally deformed rocks. Int J Earth Sci 90:77–87. doi:10.1007/s005310000152

Huang R, Audétat A (2011) A critical look at the titanium-in-quartz (TitaniQ) thermobarometer. Mineralogical Magazine Goldschmidt Abstract p 1065

Huang R, Audétat A (2012) The titanium-in-quartz (TitaniQ) thermobarometer: a critical examination and re-calibration. Geochim Cosmochim Acta 84:75–89. doi:10.1016/j.gca.2012.01.009

Jacamon F, Larsen RB (2009) Trace element evolution of quartz in the charnockitic Kleivan granite, SW-Norway: the Ge/Ti ratio of quartz as an index of igneous differentiation. Lithos 107:281–291. doi:10.1016/j.lithos.2008.10.016

Jessell MW (1987) Grain-boundary migration microstructures in a naturally deformed quartzite. J Struct Geol 9:1007

Kawasaki T, Osanai Y (2008) Empirical thermometer of TiO_2 in quartz for ultrahigh-temperature granulites of East Antarctica. Geol Soc Lond Spec Publ 308:419–430. doi:10.1144/SP308.21

Kohn MJ, Northrup CJ (2009) Taking mylonites' temperatures. Geology 37:47–50. doi:10.1130/G25081A.1

Larsen RB, Henderson I, Ihlen PM, Jacamon F (2004) Distribution and petrogenetic behaviour of trace elements in granitic pegmatite quartz from South Norway. Contrib Miner Petrol 147:615–628. doi:10.1007/s00410-004-0580-4

Martin JJ, Armington AF (1983) Effect of growth rate on quartz defects. J Cryst Growth 62:203–206

Menegon L, Nasipuri P, Stünitz H, Behrens H, Ravna E (2011) Dry and strong quartz during deformation of the lower crust in the presence of melt. J Geophys Res 116:1–23. doi:10.1029/2011JB008371

Ostapenko GT, Tarashchan AN, Mitsyuk BM (2007) Rutile-quartz geothermobarometer. Geochem Int 45:506–508. doi:10.1134/S0016702907050084

Pec M, Stünitz H, Heilbronner R (2011) Semi-brittle deformation of granitoid gouges in shear experiments at elevated pressures and temperatures. J Struct Geol 1–22. doi:10.1016/j.jsg.2011.09.001

Pennacchioni G, Menegon L, Leiss B, Nestola F, Bromiley G (2010) Development of crystallographic preferred orientation and microstructure during plastic deformation of natural coarse-grained quartz veins. J Geophys Res. doi:10.1029/2010JB007674

Perkins D (2002) Mineralogy, 2nd edn. Prentice Hall Publishers, New Jersey

Poirier J (1985) Creep of crystals. Cambridge University Press, New York

Prior DJ, Boyle AP, Brenker F, Cheadle MC, Austin D, Lopez G, Peruzzo L, Potts GJ, Reddy S, Spiess R, Timms NE, Trimby PW, Wheeler J, Zetterström L (1999) The application of electron backscatter diffraction and orientation contrast imaging in the SEM to textural problems in rocks. Am Mineral 84:1741–1759

Rankama K, Sahama TG (1950) Geochemistry. University of Chicago Press, Chicago

Rossi M, Rolland Y, Vidal O, Cox SF (2005) Geochemical variations and element transfer during shear-zone development and related episyenites at middle crust depths: insights from the Mont Blanc granite (French—Italian Alps). Geol Soc Lond Spec Publ 245:373–396. doi:10.1144/GSL.SP.2005.245.01.18

Rusk BG (2006) Intensity of quartz cathodoluminescence and trace-element content in quartz from the porphyry copper deposit at Butte, Montana. Am Mineral 91:1300–1312. doi:10.2138/am2006.1984

Rusk BG, Lowers HA, Reed MH (2008) Trace elements in hydrothermal quartz: relationships to cathodoluminescent textures and insights into vein formation. Geology 36:547. doi:10.1130/G24580A.1

Sato K, Santosh M (2007) Titanium in quartz as a record of ultrahigh-temperature metamorphism: the granulites of Karur, southern India. Mineral Mag 71:143–154. doi:10.1180/minmag.2007.071.2.143

Sinha AK, Hewitt DA, Rimstidt JD (1986) Fluid interaction and element mobility in the development of ultramylonites. Geology 14:883–886. doi:10.1130/0091-7613(1986)14<883

Smith V, Shane P, Nairn I (2010) Insights into silicic melt generation using plagioclase, quartz and melt inclusions from the caldera-forming Rotoiti eruption, Taupo volcanic zone, New Zealand. Contrib Miner Petrol 160:951–971. doi:10.1007/s00410-010-0516-0

Spear FS, Wark DA (2009) Cathodoluminescence imaging and titanium thermometry in metamorphic quartz. J Metamorph Geol 27:187–205. doi:10.1111/j.1525-1314.2009.00813.x

Stipp M, Tullis J (2003) The recrystallized grain size piezometer for quartz. Geophys Res Lett 30:1–5. doi:10.1029/2003GL018444

Stipp M, Stünitz H, Heilbronner R, Schmid SM (2002a) Dynamic recrystallization of quartz: correlation between natural and experimental deformation conditions. In: de Meer S, Drury MR, Bresser JHP, Pennock GM (eds) Deformation mechanisms, rheology and tectonics: current status and future perspectives. Special Publication, Geological Society, London 200:171–190

Stipp M, Stünitz H, Heilbronner R, Schmid SM (2002b) The eastern Tonale fault zone: a "natural laboratory" for crystal plastic deformation of quartz over a temperature range from 250 to 700 °C. J Struct Geol 24:1861–1884

Stipp M, Tullis J, Behrens H (2006) Effect of water on the dislocation creep microstructure and flow stress of quartz and implications for the recrystallized grain size piezometer. J Geophys Res 111:B04201. doi:10.1029/2005JB003852

Stipp M, Tullis J, Scherwath M, Behrmann JH (2010) A new perspective on paleopiezometry: dynamically recrystallized grain size distributions indicate mechanism changes. Geology 38:759–762. doi:10.1130/G31162.1

Storm LC, Spear FS (2009) Application of the titanium-in-quartz thermometer to pelitic migmatites from the Adirondack Highlands, New York. J Metamorph Geol 27:479–494. doi:10.1111/j.1525-1314.2009.00829.x

Stünitz H (1998) Syndeformational recrystallization: dynamic or compositionally induced? Contrib Miner Petrol 131:219–236

Stünitz H, Fitz Gerald JD, Tullis J (2003) Dislocation generation, slip systems, and dynamic recrystallization in experimentally deformed plagioclase single crystals. Tectonophysics 372:215–233. doi:10.1016/S0040-1951(03)00241-5

Tarantola A, Diamond LW, Stünitz H (2010) Modification of fluid inclusions in quartz by deviatoric stress I: experimentally induced changes in inclusion shapes and microstructures. Contrib Miner Petrol 160:825–843. doi:10.1007/s00410-010-0509-z

Tarantola A, Diamond LW, Stünitz H, Thust A, Pec M (2012) Modification of fluid inclusions in quartz by deviatoric stress. III: influence of principal stresses on inclusion density and orientation. Contrib Miner Petrol. doi:10.1007/s00410-012-0749-1

Thomas JB, Watson BE (2012) Application of the Ti-in-quartz thermobarometer to rutile-free systems. Reply to: a comment on: "TitaniQ under pressure: the effect of pressure and temperature on the solubility of Ti in quartz" by Thomas et al. Contrib Miner Petrol. doi:10.1007/s00410-012-0761-5

Thomas JB, Watson BE, Spear FS, Shemella PT, Nayak SK, Lanzirotti A (2010) TitaniQ under pressure: the effect of pressure and temperature on the solubility of Ti in quartz. Contrib Miner Petrol 160:743–759. doi:10.1007/s00410-010-0505-3

Thust A, Tarantola A, Stünitz H, Heilbronner R, Behrens H, Fitz Gerald JD (2012) Water redistribution in experimentally deformed natural quartz single crystals. PhD Thesis at university of Basel, Switzerland

Tullis TE, Tullis J (1986) Experimental rock deformation techniques. In: Hobbs BE, Heard HC (eds) Mineral and rock deformation: laboratory studies. Geophys Monogr Ser 36:297–324. AGU, Washington. doi:10.1029/GM036p0297

Urai JL, Means WD, Lister GS (1986) Dynamic recrystallization of minerals. In: Hobbs E, Heard HC (eds) Mineral and rock deformation: laboratory studies. Geophys Monogr Ser 36:161–199 AGU, Washington. doi:10.1029/GM036p0161

Vazquez JA, Kyriazis SF, Reid MR, Sehler RC, Ramos FC (2009) Thermochemical evolution of young rhyolites at Yellowstone: evidence for a cooling but periodically replenished postcaldera magma reservoir. J Volcanol Geoth Res 188:186–196. doi:10.1016/j.jvolgeores.2008.11.030

Vernooij MGC, Kunze K, Den Brok B (2006a) "Brittle" shear zones in experimentally deformed quartz single crystals. J Struct Geol 28:1292–1306. doi:10.1016/j.jsg.2006.03.018

Vernooij MGC, Den Brok B, Kunze K (2006b) Development of crystallographic preferred orientations by nucleation and growth of new grains in experimentally deformed quartz single crystals. Tectonophysics 427:35–53. doi:10.1016/j.tecto.2006.06.008

Wark DA, Watson BE (2006) TitaniQ: a titanium-in-quartz geothermometer. Contrib Miner Petrol 152:743–754. doi:10.1007/s00410-006-0132-1

Wark DA, Hildreth W, Spear FS, Cherniak DJ, Watson BE (2007) Pre-eruption recharge of the Bishop magma system. Geology 35:235. doi:10.1130/G23316A.1

Watson BE (2004) A conceptual model for near-surface kinetic controls on the trace-element and stable isotope composition of abiogenic calcite crystals. Geochim Cosmochim Acta 68:1473–1488. doi:10.1016/j.gca.2003.10.003

Watson BE, Liang Y (1995) A simple model for sector zoning in slowly grown crystals: implications for growth rate and lattice diffusion, with emphasis on accessory minerals in crustal rocks. Am Mineral 80:1179–1187

Wheeler J, Prior DJ, Jiang Z, Spiess R, Trimby PW (2001) The petrological significance of misorientations between grains. Contrib Miner Petrol 141:109–124. doi:10.1007/s004100000225

White S (1976) The effects of strain on the microstructures, fabrics, and deformation mechanisms in quartzites. Philos Trans R Soc Lond 283:69–86

Wilson CJN, Seward TM, Allan ASR, Charlier BLA, Bello L (2012) A comment on: "TitaniQ under pressure: the effect of pressure and temperature on the solubility of Ti in quartz", by Jay B. Thomas, E. Bruce Watson, Frank S. Spear, Philip T. Shemella, Saroj K. Nayak and Antonio Lanzirotti. Contrib Miner Petrol. doi:10.1007/s00410-012-0757-1